The remarkable role of metal promoters on the catalytic activity of Co-Cu based nanoparticles for boosting hydrogen evolution: Ammonia borane hydrolysis

Bilge Coşkuner Filiz*, Aysel Kantürk Figen, Sabriye Pişkin

Department of Chemical Engineering, Yıldız Technical University, İstanbul, 34210, Turkey

ABSTRACT

The development of highly efficient catalysts for hydrogen evolution has a crucial significance due to adaptation for sustainable clean energy systems. This study provides potentially powerful approach for catalytic hydrogen evolution based on ammonia borane (NH_3BH_3) hydrolysis in presence of ternary metal nanoparticles (TMNPs). Herein, we draw up a strategy by using non-noble (Ni, Ag) and noble (Ru, Pt, Pd and Rh) metal promoters in the structure of Co-Cu nanoparticles to boost their catalytic activity for hydrogen evolution by NH_3BH_3 hydrolysis. Internal and external properties of TMNPs catalysts are characterized by using XRD, SEM/EDS, FTIR, XPS, XRF, ICP-OES, BET, TEM and SAED/HRTEM techniques and performed for hydrogen evolution tests. Kinetic and thermodynamic assessments, bimolecular reaction mechanism investigation and reusability-recyclability-stability performance results relieve that Rh promoted CoCu TMNPs delivers highest hydrogen evolution activity with 21.21 l H_2 g^{-1}cat min^{-1}, 8582 mol_{H2} mol_{cat}^{-1} h^{-1} initial turnover frequency (TOF) value, and 36.50 kJ mol^{-1} activation energy (E_a) by providing the release of 3 equivalent H_2 per mole of NH_3BH_3 even after 10th use of catalytic performance tests.

1. Introduction

In recent decades, nanomaterials have been come into prominence in consequence of their properties that provide functional application fields such as catalysis [1,2]. The catalysts, play an important role in science and many industrial processes, are used to produce well over 50% of all man made products [3]. The development and uses of catalysts are a major part of the constant search for new ways of increasing product yield and selectivity from chemical reactions [4]. The catalysts are prepared by mixing two or more metal together may show better activities than on an individual basis due to synergistic effects observe by changing an internal or external properties. As with mixtures of metals, it is impossible to obtain advantageous predictions in general about changes in an activity. Impressing activity results can be recorded by testing various combinations of metals [5]. Promoting of metal nanoparticles by foreign metals is interesting and provides enormous opportunities for metal nanoparticle engineering. Promoting metal nanoparticles with atom precision is of great importance to subtly tune the properties of metal nanoparticles and gains insight into the tuning mechanism [6]. The presence of the promoter influences activity of the catalysts. On the one hand, the promoter increases dispersion of active

sites by provoking formation of undesired products. Nowadays, bimetal nanoparticles for catalytic applications widely use and come to those ternary nanoparticles by metal promoted-bi metal structures also have gained attraction. Although, the interaction between the promoting metal in bimetal nanoparticles has not been identified, the synergistic or counteractive effect has been reported by many researchers [5–10]. Scientist have also draw attention to several additives such as B [11], P [12] etc. Recently, substantial efforts have been dedicated to deep understand of the important but challenging matter in catalyst to develop enhanced and stabilize the activity.

Renewable energy-driven systems call for development of low-cost and capable catalysts for capture and storage of batch renewable energy sources. Hydrogen (H_2) has gain tremendous attention with its clean nature and high gravimetric energy density compared to various green energy carrier candidates [13]. Hydrogen can be produced from water, biomass, natural gas or coal. Nowadays, most hydrogen plants are based on nonrenewable natural resources that are not at all sustainable [14]. Supplying pure hydrogen for mobile and stationary applications at moderate temperatures, boron based chemical hydrides (such as NH_3BH_3, $NaBH_4$, $LiBH_4$, KBH_4, etc.) with high gravimetric and volumetric hydrogen storage capacities are probable contender [11,15]. For

---

* Corresponding author.
E-mail address: bilgecoskuner@gmail.com (B. Coşkuner Filiz).

implement the low cost hydrogen evolution with zero emission of greenhouse gases, ammonia borane (NH_3BH_3, AB) is considering one of the best fuel as a source of pure H_2 to supply on-board to fuel cell applications [16]. Among hydrogen storage mediums, NH_3BH_3 becomes prominent in energy systems with high hydrogen content as 19.6 wt.%, stability under atmospheric conditions, nontoxicity, high solubility and stability in water [11]. By using proper catalyst, efficient hydrogen evolution 3 mol per mol of NH_3BH_3 has been achieved. Noble and non-noble catalysts have been developed for this aim by scientists. Besides, noble metals provided the highest activity for hydrolysis of NH_3BH_3, non-noble metals have been delivered cost-effective and promising alternative to pure hydrogen generation [15,17,18]. Single metal catalysts have been developed and cobalt showed noticeable catalytic activity for hydrogen evolution compared with other metals [19–21]. Later on, bimetal catalyst has gain attention due to their enhanced properties in terms of hydrogen generation activities. It is reported that metallic systems generally show improved catalytic kinetics rather than single metal catalysts due to synergistic impacts on structure of bimetal systems as Co-Cu, Co-Ni, Cu-Ni [18,21,22]. Song et.al underlined that rapid hydrolytic dehydrogenation of NH_3BH_3 at mild temperatures could be achieved by using a Co and Cu non-noble metals together with in the catalyst structure. Despite, monometallic Cu-based nanocatalysts showed low catalytic kinetics of hydrogen generation and only a little gas was released from NH_3BH_3, the superior catalytic performance of $Cu_{0.2}Co_{0.8}$/PDArGO to that of Co/PDA-rGO was ascribed to the synergistic interaction between Cu and Co according to their research [22]. The catalytic performance of bimetallic catalysts depend on their synergism that strongly relates with molar ratios of individual metals in catalyst structure [12,23].

Recently, a newly developed strategy to assemble tri-component catalyst has been remarked by performing boosted performance by far from others [12,24]. It should be underlined that activity of catalyst affect from futures such as nanoparticle size, electronic features, composition and additives into its structure and designing of favorable catalyst for NH_3BH_3 hydrolysis further investigation is required to meet the practical application criteria in terms of efficiency, cost and reusability [23,25]. Liu et al. have developed NiPtP NPs and found excellent catalytic performance for hydrous hydrazine dehydrogenation by synergistic and catalytic active surface area's increasing effect of P addition [12]. The excellent catalytic performance for reactions can be attributed to the existence of components to benefit the formation of the electron rich surface via electron transfer and smaller active sites [23].

The objectives of this study are to develop highly active and cost effective CoCu TMNPs with well-defined nanostructures by partial substitution of non-noble (Ni, Ag) and noble (Ru, Pt, Pd and Rh) metals and illuminate the promoting impact on hydrogen evolution by NH_3BH_3 hydrolysis reaction. The dependence between TMNPs structure and activity was examined by several internal and external analysis techniques. As a final step, a comparison of catalytic activity for hydrogen evolution from NH_3BH_3 was carried out and superficial active TMNPs was subject to further characterizations and performances.

2. Experimental section

2.1. Synthesis and characterization of ternary metal nanoparticles

Ternary metal nanoparticles (TMNPs) in theoretical structure of $Co_{0.495}Cu_{0.495}X_{0.01}$ were synthesized by sol-gel procedure followed by nitrate-combustion method. A certain amount of citric acid ($C_6H_8O_7.H_2O$, Merck) as an organic ligand/fuel in the synthesis solution was dissolved in distillated water to obtain 0.2 M aqueous sol. As starting materials, appropriate amount of cobalt(II)nitrate hexahydrate ($Co(NO_3)_2·6H_2O$, Merck, %97), copper(II)nitrate hexahydrate (Cu $(NO_3)_2·6H_2O$, Merck, %97) and third metal salt (nickel(II)chloride hexahydrate ($NiCl_2·6H_2O$, Merck, > %98), silver nitrate ($AgNO_3$,

Merck, extra pure), ruthenium(III) chloride hydrate ($RuCl_3·H_2O$, Merck), chloroplatinic acid hexahydrate ($H_2PtCl_6·6H_2O$, Merck, %40 Pt), palladium(II) chloride ($PdCl_2$, Merck, %59 Pd), rhodium(III) chloride trihydrate ($RhCl_3·3H_2O$, Merck, %38 Rh)) were added into sol rapidly. After stirring (500 rpm) at 80 °C to form a gel structure, the materials were dried in an incubator overnight. The obtained powder was then subjected to a nitrate-combustion procedure at 450 °C for 4 h under an oxidative atmosphere and then an internal and external characterizations were carried out as given below.

The crystalline structures of TMNPs were identified by Powder X-ray diffraction (XRD) analysis, performed on Philips Panalytical X'Pert-Pro diffractometer with a CuKα source (40 mA and 45 kV). Based on XRD analysis data, Scherrer-Debye equation was used to calculate the crystalline particle sizes of TMNPs. Chemical structures of TMNPs were analyzed via Fourier transform infrared spectroscopy (FTIR, Perkin Elmer Spectrum One) equipped with attenuated total reflection (ATR). The specific areas and properties such as pore size distrubition of TMNPs were measured by multipoint conventional Brunauer, Emmett and Teller (BET) method, which numerical values were calculated from relative pressure p/p° of 0-0.5 by nitrogen adsorption at liquid nitrogen temperature using volumetric surface analyzer (Micrometerics Co, USA). Elemental contents of TMNPs were determined by X-ray fluorescence (XRF) technique (Minipal4-Panalytical) with "STANDARDLESS" analysis software and inductively coupled plasma optical emission spectrometry (ICP/OES, Perkin Elmer, Optima 2100 DV). The morphologies and elemental mapping of all the nanoparticles were observed a using CamScan scanning electron microscope (SEM) equipped with energy dispersive spectroscopy (EDS). The chemical composition characterization was performed by X-ray photoemission spectra (XPS) via a Thermo Scientific K-Alpha spectrometer by using an Aluminum anode (Al Kα = 1468.3 eV) at an electron take-off angle of 90° between the sample surface and the axis of the analyzer lens. The XPS spectra were recorded using an Avantage 5.9 data system. The binding energy scale was calibrated by assigning the C 1 s signal at 284.5 eV.

In our previous study, we synthesized and characterized the $Co_{0.5}Cu_{0.5}$ NPs (7.26 $m^2 g^{-1}$ BET surface area, 0.04 $cm^3 g^{-1}$ pore volume and 21.52 nm pore diameter) and the results of metal promoted CoCu TMNPs were compared [21].

2.2. Hydrogen evolution during NH_3BH_3 hydrolysis over TMNPs

Hydrogen evolution during NH_3BH_3 hydrolysis over TMNPs was performed based on water displacement method. The reactor containing 0.12 M NH_3BH_3 (Aldrich, %97) aqueous solution was immersed into water bath controlled with temperature controller (± 2 °C) and stirred with magnetic system (750 rpm). The evolved hydrogen gas collected into burette, measured and recorded by a chronometer as a function of time. Hydrogen evolution rates (HER, l $H_2 g^{-1}cat min^{-1}$) in the presence of TMNPs catalysts (5 mg) were calculated by using hydrogen evolution profiles obtained at a specific temperature of 60 °C, as specified by the U.S. DOE targets for onboard hydrogen storage systems in light-duty vehicles [26]. The collected data was used to calculate HER and determination of activity of TMNPs.

In order to investigate the temperature effect on HER, hydrogen evolution performances were tested at different temperatures (22 °C–80 °C ± 2 °C) and in 0.12 M NH_3BH_3 in the presence of 5 mg TMNPs. For making compassion, changes in HER were calculated in percentages respect to CoCu's HER value at the same temperature based on the following equation:

$$HER\ Change\ (\%) = \frac{HER_{promoted} - HER_{CoCu}}{HER_{CoCu}} \times 100 \tag{1}$$

2.3. Kinetic and thermodynamic assessment

The kinetic and thermodynamic assessments of hydrogen evolution during NH_3BH_3 hydrolysis over TMNPs were performed based on Power Law Kinetic Models (Zero, First and Second), Arrhenius and Eyring approaches. The series of hydrogen evolution were carried out at 22 °C–80 °C ± 2 °C as described in Section 2.2. The volumetric hydrogen evolution was converted to molar equivalent and NH_3BH_3 concentration ($C_{NH_3BH_3}$, M) as a function of time (t, min) and used to determine correlation co-factors (R^2), kinetic and thermodynamic values. Kinetic values as apparent activation energy (E_a, kJ mol^{-1}), rate constant (k) and thermodynamic values as activation enthalpy ($\Delta H^{\neq}$, kJ mol^{-1}) and entropy ($\Delta S^{\neq}$, J mol^{-1}) were calculated from Arrhenius and Eyring plots as given Eqs. (2) and (3). Also Gibbs free energy ($\Delta G^{\neq}$, kJ mol^{-1}) was calculated from general thermodynamic equation from $\Delta H^{\neq}$ and $\Delta S^{\neq}$ values for 22 °C (Eq. (4)).

$$\ln(k) = \ln(k_0) + \frac{E_a}{RT} \tag{2}$$

$$\ln\left(\frac{k}{T}\right) = \ln\left(\frac{k_B}{h}\right) + \frac{\Delta S}{R} - \frac{\Delta H}{R} \cdot \frac{1}{T} \tag{3}$$

$$\Delta G^{\neq} = \Delta H^{\neq} - T \cdot \Delta S^{\neq} \tag{4}$$

where k_0, R, k_B and h were Arrhenius, Universal gas, Boltzmann and Planck constants, respectively [2,3].

2.4. Further characterization of most active TMPNs

2.4.1. Structural characterization

Further morphological characterization of TMNPs with best activity was subject to transmission electron microscopy (TEM, JEOL JEM 1400 Plus) analysis. Also the adsorption isotherms and pore distribution of TMNPs measured by nitrogen adsorption at liquid nitrogen temperature using volumetric surface analyzer (Micrometerics Co, USA). High resolution transmission electron microscopy (HRTEM) and selected area electron diffraction (SAED) investigations were performed on JEOL JEM 2100 HRTEM operating at 200 kV. Images were taken by Gatan Model 794 Slow Scan CCD Camera and also by Gatan Model 833 Orius SC200D CCD Camera. Carbon support film coated copper TEM grids (Electron Microscopy Sciences, CF200-Cu, 200 mesh) were used.

2.4.2. Bimolecular reaction mechanism investigation

Better understanding of TMPNs-NH_3BH_3 interaction, more complex kinetic approach was used, namely Langmuir-Hinshelwood (L-H). In heterogeneous catalysis systems, bimolecular reaction mechanism provides more information about mechanism of the reactions. This approach firstly takes into consideration of adsorption of both reactants over catalyst surface and then reaction occurs on the active sites of catalyst. Also adsorption constant (K_a) was calculated based on equations [5–7] given below. According to results bimolecular reaction mechanism was proposed [4].

$$\frac{dC_{NH_3BH_3}}{dt} = -r_{NH_3BH_3} = -k \frac{K_a C_{NH_3BH_3}}{1 + K_a C_{NH_3BH_3}} \tag{5}$$

$$min_{K_a} f(K_a) = (1 - R^2_{22°C}) + (1 - R^2_{40°C}) \tag{6}$$

$$\frac{1}{K_a} \ln\left(\frac{C_{NH_3BH_3o}}{C_{NH_3BH_3}}\right) + (C_{NH_3BH_3o} - C_{NH_3BH_3}) = k \cdot t \tag{7}$$

2.4.3. Reusability, recyclability, stability performances

To check reusability, recyclability and stability performances of the as-prepared TMNPs, the hydrolysis reaction was repeated 10 times under conditions as 0.12 M NH_3BH_3 aqueous solution, 5 mg TMPNs, 60 °C and 750 rpm. For reusability performance, after the first run the TMNPs was collected and washed with water and acetone, and then dried at 110 °C in a vacuum oven over night. Subsequently, freshly-prepared 0.12 M NH_3BH_3 solution was mixed with the recovered catalyst, and a new run of the catalytic reaction was started. For recyclability performance, following first run without any procedure, used TMNPs and spent solution was maintained and only 1.2 mmol NH_3BH_3 was re-added into batch reactor for starting a new run. For stability performance, after first run used TMNPs was stored in spent fuel under dark medium for 3 months. After this period of time, the reaction was performed by re-addition of 1.2 mmol NH_3BH_3 into spent solution. The data was collected until no H_2 was evolved that was used to calculate hydrogen evaluation rate (HER, l H_2 min^{-1} g^{-1} catalyst) and determination of change in activity of TMNPs. After the reusability, recyclability, stability performances, the used catalysts were isolated from the spent reaction solutions for morphological characterization by SEM analysis.

2.4.4. Effect of NH_3BH_3 concentration and catalyst dosage

Hydrogen evolution at different NH_3BH_3 concentrations –from 0.12 M to 1.20 M- were also studied in the presence of TMPNs catalyst (5 mg) at 60 °C and 750 rpm. Also the effect of the TMPNs amount on the hydrogen evolution was investigated by altering the catalyst dosage from 1.25 mg to 10 mg under conditions as 0.12 M NH_3BH_3, 60 °C and 750 rpm.

3. Results and discussion

3.1. Characterization of ternary metal nanoparticles

Fig. 1 represents the SEM images (a–f), XRD patterns (g) and FTIR spectrums (h) of corresponding ternary metal nanoparticles. All the TMNPs showed similar particle-like morphology with particles having spherical shape and size in a range of 30–50 nm as certained by SEM. The successful synthesis of Co-Cu based TMNPs was firstly verified by XRD analysis. In the XRD patterns of all TMNPs, Cu was found in two type in the structure. The characterized main peaks were obtained at 31.38° (220), 36.98° (311) and 65.49° (440) attributed to $Co_{2.24}Cu_{0.76}O_4$ (JCPDS:01-076-1886). There were also other peaks were belonged with CuO (JCPDS:00-041-0254) phase in all nanoparticle crystal structures. Crystal sizes of both phases were calculated based on Scherrer-Debye equation and details were given in Table 1. Defined Co-Cu-O and Cu-O phases' crystalline sizes were in the range of 22–32 nm. Additionally, no apparent diffraction was detected for third metal content of TMNPs. It was unable to provide accessible information about their crystalline structure by XRD analysis due to very low concentration of them. It was concluded that the type of promoter did not affect the main crystalline structure of TMNPs. Among all the TMNPs, which were functionalized with citric acid as an organic ligand/fuel in the synthesis solution in nitrate combustion method, exhibited no functional chemical bounds after combustion of carboxylic groups at 450 °C according to the FTIR spectrum. These results showed that in procedure of TMNPs preparations by nitrate-combustion method, citric acid as an efficient organic ligand/fuel was preferred which cause the rapid reduction of metal ions to oxide forms by combustion and thus it did not permit the particles to grow above a few nanometers.

Table 1 also listed quantitative elemental analyses results obtained from XRF, ICP-OES and SEM-EDS. In order to investigate the effect of metal promoter on catalytic activity, TMNPs were synthesized by straightforward preparation to demonstrate the third metal by verified it (as Rh, Pd, etc.) in theoretical single molar ratio (0.01). The proposed molar ratios were achieved successfully and promoters uniformly distributed through the TMNPs structure according to the chemical composition and elemental mapping results. Almost same concentration of metals on the surface and bulk structure was obtained, as evidenced by also the corresponding EDS mappings (see Fig. 2). The chemical composition results showed that desired nanostructures were developed by target content, and furthermore, uniform element distribution
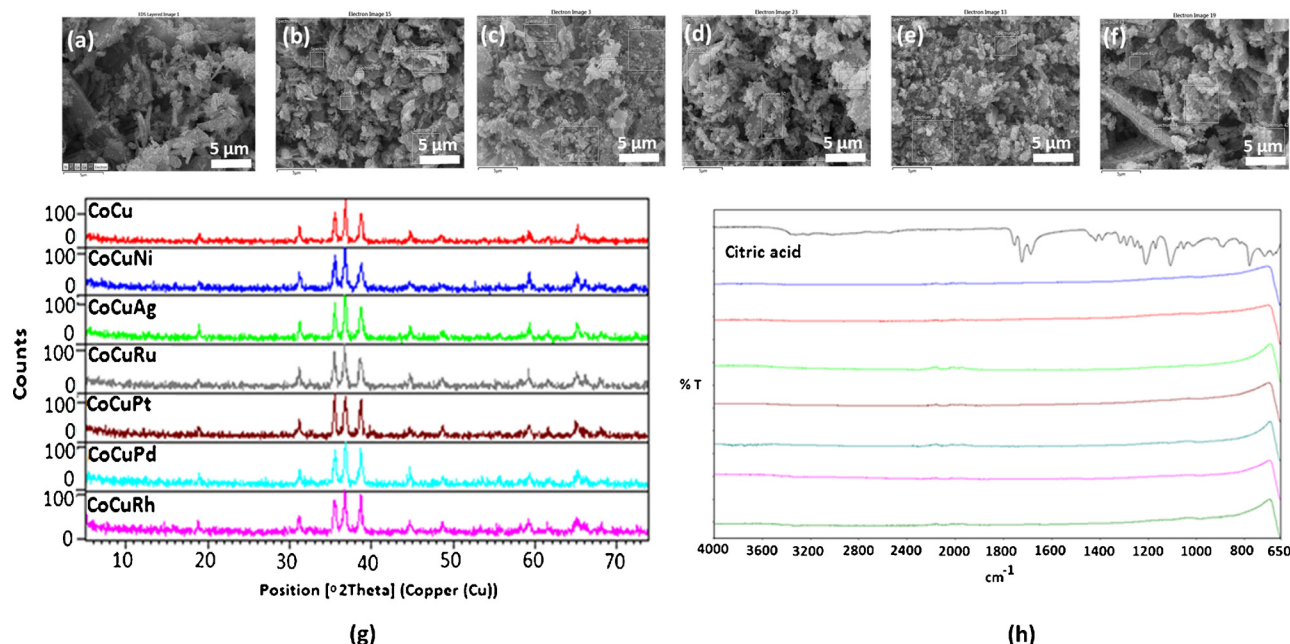
Fig. 1. Structural characterization of TMNPs: SEM images of (a) CoCuNi, (b) CoCuAg, (c) CoCuRu, (d) CoCuPt, (e) CoCuPd, (f) CoCuRh at 5000x, (g) XRD patterns of Co-Cu based catalyst and TMNPs, (h) FT-IR spectra of citric acid and TMNPs.

throughout TMNPs were controlled via sol-gel method. BET surface area of all TMNPs were analyzed via nitrogen adsorption and also reported in Table 1. The trend in the surface area increased in following order: Ru > Ni > Rh > Ag > Pt > Pd, also pore volume had the same tendency. This result showed that surface area of the TMNPs was independent from metals promoter type whenever it was noble or non-noble metal.

Fig. 3 shows the XPS measurement spectra of all TMNPs to get in-depth understanding of the electronic structure of surfaces and investigation of effect on interaction between promoters and CoCu: survey (a), Co 2p (b), Cu 1 s (c), promoters' electron states as Ag 3d, Ni 2p, Ru 3p, Pt 4d, Pd 3d, Rh 3d (d), O 1 s (e). The survey spectra was in the 0–1350 eV of binding energy range were performed to qualitative analyses. Basically, whole scanning spectra of CoCu showed the existence of Co, Cu and O. The peaks observed at binding energies of 779.38 eV and 794.48 eV were assigned to $2p_{3/2}$ and $2p_{1/2}$ core levels of Co in CoCu NPs oxide structure, respectively. The Cu 2p core level spectrum represented two strong peaks in 933.08 eV and 953.08 eV, confirmed the oxide nature of Cu in agreement with XRD results. Binding energy of O 1 $s_{1/2}$ were 529.18 eV and 530.98 eV assumed that metals atoms existed in the catalyst with oxygen bound on surface [21].

To clarify the electronic structures and their bonding behaviors, the binding energy of promoters (Ni, Ag, Ru, Pt, Pd and Rh) were also measured by XPS analyses and Fig. 3b–e exhibited the high resolution spectra of Co 2p, Cu 1 s, promoters and O 1 s, respectively. All the spectras clearly demonstrated successfully incorporation of promoters in the crystal structure. The promoter addition changed the electronic environment of the Co-Cu structure and it was obtained a shift in Co $2p_{3/2}$ by 0.4 eV for CoCuNi, CoCuAg, CoCuPt, CoCuPd, CoCuRh and 0.3 eV for CoCuRu TMNPs towards higher binding energies. Comparison with non-promoted CoCu TMNPs implied neat charge transfer from Co-Cu to promoters and this transformation led to electron rich promoters specimens due to net differences in their electron negativity values (Co:1.88, Cu:1.9, Ni:1.91, Ag: 1.93, Pd: 2.2, Ru: 2.2, Pt: 2.28, Rh: 2.28) [24]. Moreover this, Rh promoted CoCu NPs became more electron rich in comparison with CoCu and other TMNPS. It was possible to correlate the activity of the catalyst with changing in the binding energy towards higher values by promoting of CoCu catalyst. Jia et al. [27] prepared the modified Au based catalyst and reported that addition into structure changed the electronic level, enhanced the interaction between active species and supported that resulting with improvement of catalytic activity [27]. Ni 2p spectrum was attributable to

Table 1
Characterization results of metal promoted CoCu TMNPs.

Properties	Analyses		TMNPs					
			CoCuNi	CoCuAg	CoCuRu	CoCuPt	CoCuPd	CoCuRh
Qualitative Crystal structure	Phases (JCPDS), % and Size	Co$_{2.24}$Cu$_{0.76}$O$_4$ (01-076-1886)	22.08 nm	27.50 nm	29.41 nm	29.42 nm	32.04 nm	25.64 nm
		CuO (00-041-0254)	30.71 nm	23.66 nm	27.34 nm	28.86 nm	26.76 nm	30.60 nm
Chemical Composition	XRF, mol:mol:mol		0.48:0.51:0.01	0.49:0.50:0.01	0.49:0.50:0.01	0.49:0.50:0.01	0.49:0.50:0.01	0.49:0.50:0.01
	ICP-OES, mol:mol:mol		0.48:0.51:0.01	0.49:0.50:0.02	0.49:0.50:0.01	0.49:0.50:0.01	0.49:0.50:0.01	0.49:0.50:0.01
	SEM/EDS, mol:mol:mol		0.48:0.51:0.01	0.51:0.48:0.01	0.49:0.50:0.01	0.47:0.52:0.01	0.48:0.51:0.01	0.46:0.53:0.01
	Average composition, mol:mol:mol		0.480:0.510:0.010	0.497:0.493:0.013	0.490:0.500:0.010	0.483:0.507:0.010	0.487:0.503:0.010	0.480:0.510:0.01
Surface	BET Spesific Surface Area, m^2. g^{-1}		11.28	7.51	13.45	6.16	5.80	10.68
	Pore volume, cm^3. g^{-1}		0.07	0.04	0.09	0.04	0.04	0.06
	Pore diameter, nm		24.27	21.56	26.12	27.18	30.69	21.88
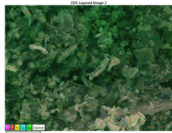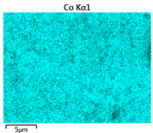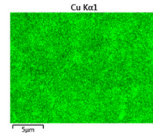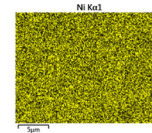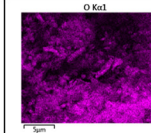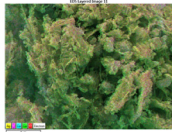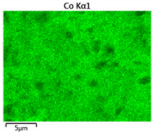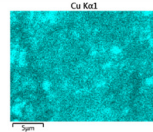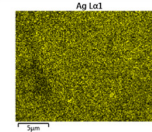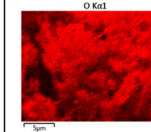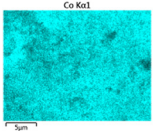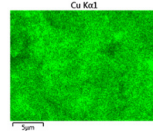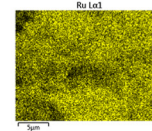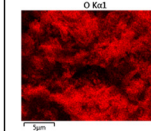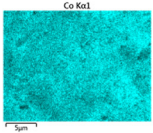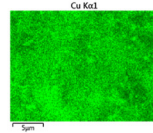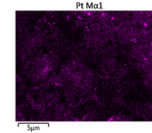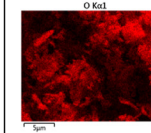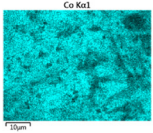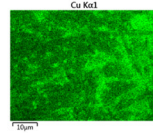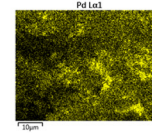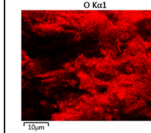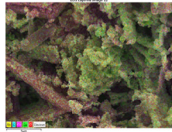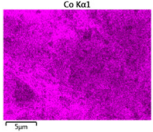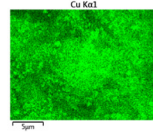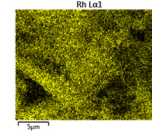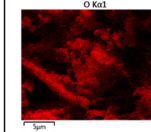
TMNPs	Elemental Mapping	Co Kα1	Cu Kα1	X Kα1	O Kα1
CoCuNi		Co Kα1	Cu Kα1	Ni Kα1	O Kα1
CoCuAg		Co Kα1	Cu Kα1	Ag Lα1	O Kα1
CoCuRu		Co Kα1	Cu Kα1	Ru Lα1	O Kα1
CoCuPt		Co Kα1	Cu Kα1	Pt Mα1	O Kα1
CoCuPd		Co Kα1	Cu Kα1	Pd Lα1	O Kα1
CoCuRh		Co Kα1	Cu Kα1	Rh Lα1	O Kα1

Fig. 2. Elemetal mapping results of TMNPs at 5000x: (a) CoCuNi, (b) CoCuAg, (c) CoCuRu, (d) CoCuPt, (e) CoCuPd, (f) CoCuRh.
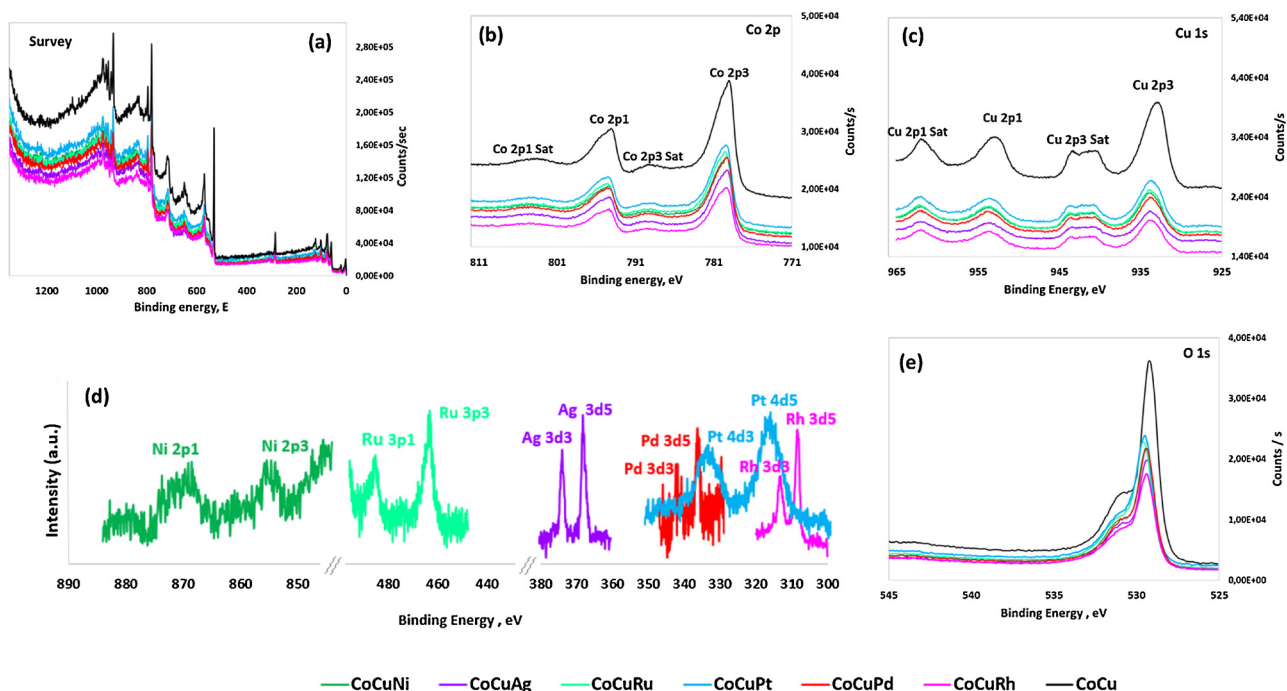
Fig. 3. X-ray photoelectron spectra of metal promoted CoCu TMNPs: (a) survey, (b) Co 2p, (c) Cu 1 s, (d) promoters' electron states as Ag 3d, Ni 2p, Ru 3p, Pt 4d, Pd 3d, Rh 3d, (e) O 1 s.
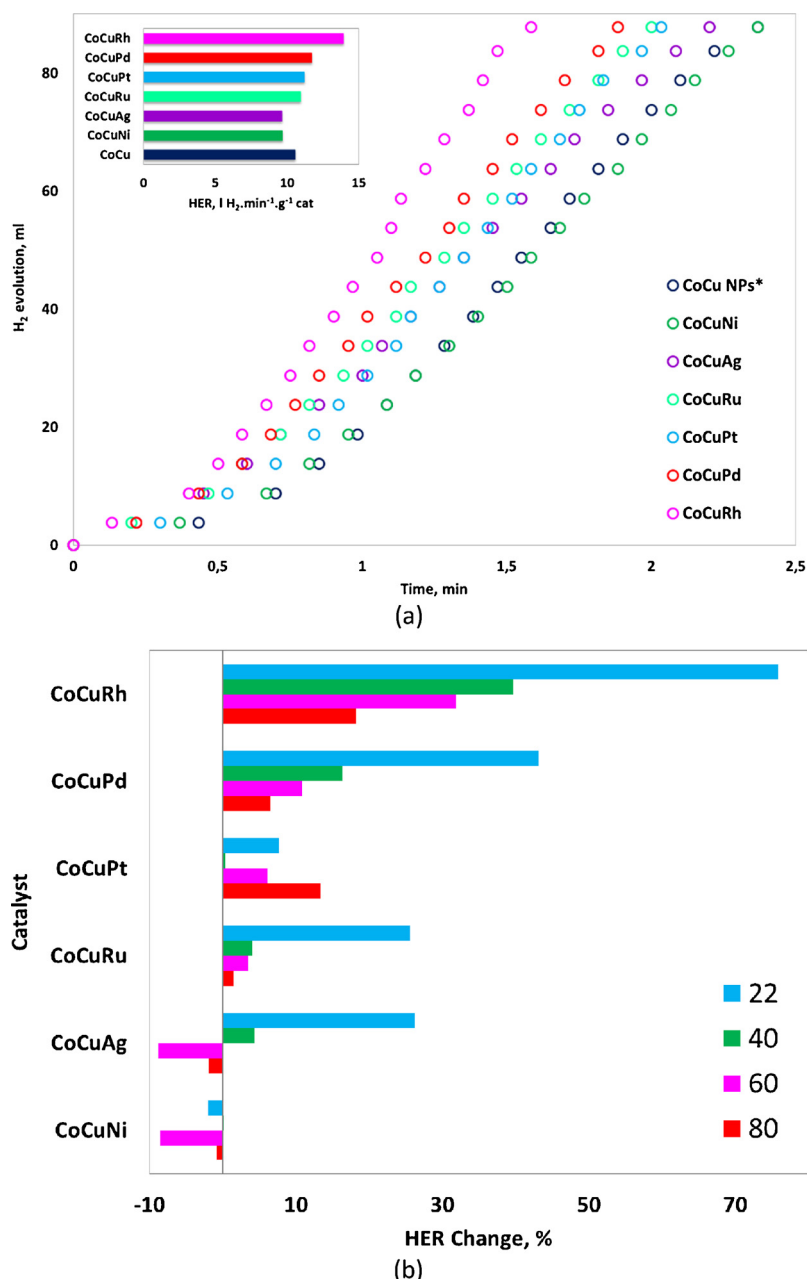
Fig. 4. Hydrogen evolution over TMNPs catalysts (CoCuNi, CoCuAg, CoCuRu, CoCuPt, CoCuPd, CoCuRh): 0.12 M NH_3BH_3 aqueous solution, 5 mg catalyst, 750 rpm stirring rate: (a) Hydrogen evolution profiles and rates (inset) at 60 °C, (b) Comparison bars of HER changes (%) in HER at different hydrolysis temperatures (22-80 °C).

oxidized Ni^{2+} species peaks detected at 854.78 eV and 870.38 eV for Ni $2p_{3/2}$ and Ni $2p_{1/2}$ of NiO, respectively [28]. The binding energies of the Ag $3d_{3/2}$ and $3d_{5/2}$ peaks at 367.68 eV and 373.08 eV could be indexed as the oxidation state of Ag^{1+} [29]. The peaks around the 463.95 eV and 486.88 eV were due to Ru^{2+} ions of Ru $3p_{3/2}$ and $Ru3p_{1/2}$, respectively [30]. Two sets of peaks at 316.78 eV and 333.08 eV were assigned to Pt $4d_{5/2}$ and $4d_{3/2}$, respectively confirming the presence of chemical environment of Pt^{2+} ions in sample [31]. The Pd $3d_{5/2}$ peak at 336.98 eV and Pd $3d_{3/2}$ peak at 342.38 eV were attributed to Pd(II) [32]. The measured binding energies for Rh components centered around 308.48 eV in which correspond to $3d_{5/2}$. The energy differences between the $3d_{3/2}$ and $3d_{5/2}$ peaks were at the value of 4.8 eV. As well as 308.48 eV correspond to the oxidic Rh^{3+} chemical environment [33]. It was confirmed by the XPS results, the promoter addition changed the electronic environment of the Co-Cu structure and higher

binding energies of each counterpart were detected in the electronic states of TMNPs, similar to literature [20,34].

3.2. Hydrogen evolution during NH_3BH_3 hydrolysis over TMNPs

Fig. 4 illustrates the NH_3BH_3 hydrolysis characteristics over TMNPs catalysts: (a) hydrogen evolution (ml) against to time at 60 °C and inset shows the HER, (b) changes (%) in HER respect to CoCu NPs at different hydrolysis temperatures (22–80 °C).

Fig. 4a shows profiles and rates (see inset) of hydrogen evolution during NH_3BH_3 hydrolysis over TMNPs at 60 °C by comparing CoCu NPs indexed with * [21]. Here, we presented the most relevant results to understand the boosting effect of each metal promoter, before the detailed investigation on the kinetics of the catalytic hydrogen evolution during NH_3BH_3 hydrolysis. Rh promoted CoCu TMNPs provided

the lowest reaction completion time and highest HER. As the noble metal led to increase in catalytic activity, non-noble metal content slowed down the hydrogen evolution over TMNPs. Owing to the higher reactivity of Rh, Pd, Pt and Ru promoted TMNPs in comparison with CoCu NPs, they boosted removal of hydrogen from NH_3BH_3: the order of HER was Rh > Pd > Pt > Ru. Moreover, the results for TMNPs catalysts were compared with Co NPs, Cu NPs and CoCu NPs, the hydrogen evolution activities for the hydrolysis of NH_3BH_3 in terms of HER reported as $3.56\,l\,H_2\,g^{-1}cat\,min^{-1}$, $0.42\,l\,H_2\,g^{-1}cat\,min^{-1}$, $10.56\,l\,H_2\,g^{-1}cat\,min^{-1}$ in our previous studies [19,21]. It was deduced that using metal together within the structure improving activity, even minor quantity of promoter in structure was also enhanced the catalytic properties of nanoparticles for hydrolysis of NH_3BH_3.

Fig. 4b, shows the comparison bars of HER changes (%) based on temperature increasing. The catalytic activity gradually increased with increase in hydrolysis temperature. Based on the influence of the catalyst-NH_3BH_3 interaction, higher hydrolysis rate of NH_3BH_3 were achieved with Rh, Pd, and Ru noble metals by increasing temperature. At higher temperatures about 60–80 °C and especially regarding in presence of CoCuAg and CoCuNi TMNPs, the HER change (%) showed negative values means that Ag and Ni showed slowing down effect on the reaction rate. It was also worth mentioning that the activity of CoCuAg TMNPs was almost closed to that of CoCuNi TMNPs, in spite of the fact that their activities were below reference CoCu NPs. These behavior has been also explained by previous studies in terms of the inactive characteristic of mono/bimetallic form of Ni catalyst for NH_3BH_3 dehydrogenation [19,21] and easily agglomeration of Ag counterparts [35]. Pt promoted TMNPs also increased HER as expected, but the percentage of increase has been found to be lower at low temperatures (22–40 °C). The highest HER was achieved at 80 °C over CoCuRh. The corresponding bars of CoCuRh TMNPs at 22 °C was much longer than that of other nanoparticles means that the maximum level as %76 of HER was increased by Rh promoting. This TMNPs performed significantly superior among all results. Ag and Ni promoted TMNPs did not enhanced the catalytic activity compared with un-promoted CoCu NPs and in contrast to promoting of Ru, Pt, Pd and Rh. In general trend, noble metal containing TMNPs showed improved activity than Co-CuNPs, while non-noble metal containing NPs were less active.

3.3. Kinetic and thermodynamic assessment

The aforementioned results provided strong evidence of noble metal as a third counterpart in the structure of nanoparticles boosted hydrogen evolution during NH_3BH_3 hydrolysis. This could be resulting in strong adsorption of NH_3BH_3 on catalytic sites, which could effectively activate the B−N bonds, hence decreasing the reaction energy barrier and boosting hydrogen evolution [36]. An understanding of how third metal change in structure factored into the catalytic behavior was provided by a comparison of kinetic and thermodynamic parameters. The H_2O concentration could be almost neglected due to H_2O was in large excess in hydrolysis medium. For this reason, this suggests a zero, first and second-order reaction with respect to NH_3BH_3 was

investigated [37].

Table 2 listed all kinetic and thermodynamic assessments results. All the TMNPs nearly showed zero-order reaction kinetics with respect to NH_3BH_3 concentration in hydrolysis medium (Fig. S1). It means that hydrogen evolution was independent of NH_3BH_3 concentration in reaction medium during hydrolysis reaction.

Fig. 5 shows zero-order reaction kinetic model plots for hydrolysis of NH_3BH_3 over metal promoted TMNP at different temperatures and reaction rate constants were calculated from their slope of straight-lines to obtain Arrhenius plots (see Fig. 5 inset) for each. The apparent activation energy values, from slope of Arrhenius plots, were respectively calculated as 41.54, 37.75, 38.92, 43.06, 37.81 and 36.50 kJ mol^{-1} for CoCuNi, CoCuAg, CoCuRu, CoCuPt, CoCuPd, CoCuRh. The fastest hydrogen evolution and lowest E_a value were obtained for CoCuRh TMNPs catalyzed NH_3BH_3 hydrolysis. It indicated that HER in presence of CoCuRh TMNPs was less affected by reaction medium temperatures compared with others. This caused to underline another important factor responsible for the highest HER of the CoCuRh TMNPs.

Fig. 6 shows the kinetic (a) and thermodynamic (b) assessment results for all metal promoted TMNPs. Fig. 6a shows a comparison of the apparent activation energies for hydrogen evolution from NH_3BH_3 in presence different metal promoted TMNPs in oxides state. E_a between different catalysts were ranging from 36.50 kJ mol^{-1} to 43.06 kJ mol^{-1}. This result was reasonable based on the corresponding reaction mechanism associated with change of E_a and comparable with reported values in literature as 56.3 kJ mol^{-1} for PtRu@PVP [38], 51.3 kJ mol^{-1} for $Cu_{0.2}@Co_{0.8}$/rGO [39], 51.9 kJ mol^{-1} for CoCu NPs [40], 36.08 kJ mol^{-1} for Cu@CoNi [41], 41.7 kJ mol^{-1} for $Cu_{0.2}Co_{0.8}$ [42], 41.5 kJ mol^{-1} for $Co_{0.32}@Pt_{0.68}$/C [43], 37.18 kJ mol^{-1} for Ni-Ru alloy [44], 39 kJ mol^{-1} for $Pt_{0.65}Ni_{0.35}$ [45], 42 kJ mol^{-1} for Pd°/$CoFe_2O_4$ [46]. Considering the NH_3BH_3 hydrolysis over TMNPs follows zero-order kinetics, thermodynamic parameters were also evaluated with the help of Eyrings plots (Figs. 6b and S2).$\Delta H^{\neq}$ (kJ mol^{-1}) values were between 40.38 kJ mol^{-1} and 33.83 kJ mol^{-1} that could be comparable with previous literature results as 51 ± 2 kJ mol^{-1} for RuNPs@nano-Hap [47], 43 ± 3 kJ mol^{-1} for PVP-stabilized cobalt(0) nanoclusters [48], 52 ± 2 kJ mol^{-1} for PSSA-co-MA stabilized ruthenium(0) [49], and 42 ± 2 kJ mol^{-1} for PSSA-co-MA stabilized palladium(0) nanoclusters [49]. In addition to this result, $\Delta S^{\neq}$ values were determined between -165.92 J K^{-1} mol^{-1} and -106.9 J K^{-1} mol^{-1} that could be comparable result with previous findings as: -51 ± 5 J K^{-1} mol^{-1} for RuNPs@nano-Hap [47], -126 ± 3 J K^{-1} mol^{-1} for PVP-stabilized cobalt(0) nanoclusters [48], -92 ± 2 J K^{-1} mol^{-1} for PSSA-co-MA stabilized ruthenium(0) [49] and -113 $\pm$ 3 J K^{-1} mol^{-1} for PSSA-co-MA stabilized palladium(0) nanoclusters [49]. All obtained $\Delta H^{\neq}$ (kJ mol^{-1}) and $\Delta G^{\neq}_{295}$ (kJ mol^{-1}) displayed positive and $\Delta S^{\neq}$ (J K^{-1} mol^{-1}) was negative values that demonstrating this hydrolysis reaction over TMNPs was non-spontaneous, endergonic and reagents required an external energy for leveling up the reaction to transition state. And also negative value of $\Delta S^{\neq}$ indicated that TMNPs-reactant complex had a more ordered state than the reactants in the ground state structure. Based on the transition state theory, the catalyst reduced the potential

Table 2
Kinetic model investigation at 60 °C and model values in terms of kinetic and thermodynamic parameters (The best fitting model was indicated by bold characters).

TMNPs	Kinetic model investigation R^2 values of nth degree Power Law Models			Model Values Kinetic and Thermodynamic Parameters				
	0.	1.	2.	E_a, kJ. mol^{-1}	ln(k_0), min^{-1}	$\Delta H^{\neq}$, kJ. mol^{-1}	$\Delta S^{\neq}$, J. K^{-1}. mol^{-1}	$\Delta G^{\neq}_{295}$, kJ. K^{-1}. mol^{-1}
CoCuNi	**0.9948**	0.8839	0.6352	41.54	12.09	38.86	−153.37	84.10
CoCuAg	**0.9954**	0.8969	0.6579	37.75	10.75	35.08	−164.55	83.62
CoCuRu	**0.9960**	0.8977	0.6578	38.92	11.22	36.24	−160.60	83.62
CoCuPt	**0.9921**	0.8807	0.6334	43.06	12.76	40.38	−147.81	83.98
CoCuPd	**0.9967**	0.8972	0.6545	37.81	10.89	37.81	−106.97	69.37
CoCuRh	**0.9946**	0.8860	0.6392	36.50	10.58	33.83	−165.92	82.78

Fig. 5. Zero order reaction kinetic models for hydrolysis of NH_3BH_3 over metal promoted TMNP: (a) CoCuNi, (b) CoCuAg, (c) CoCuRu, (d) CoCuPt, (e) CoCuPd, (f) CoCuRh. Insets showed the Arrhenius graphics for each.
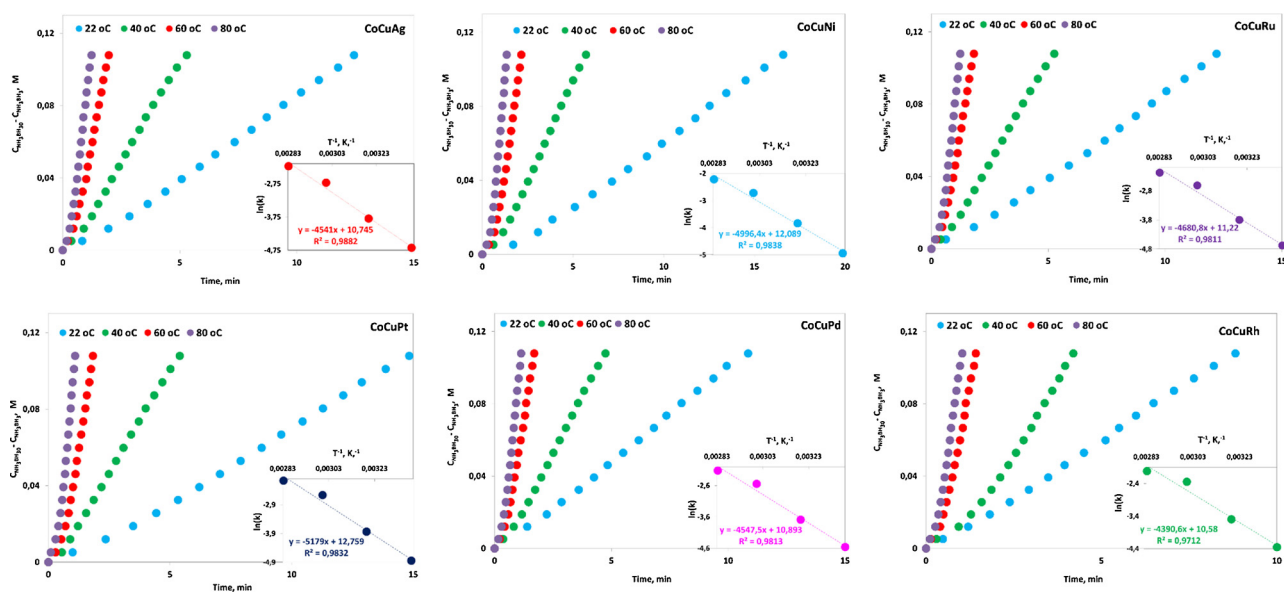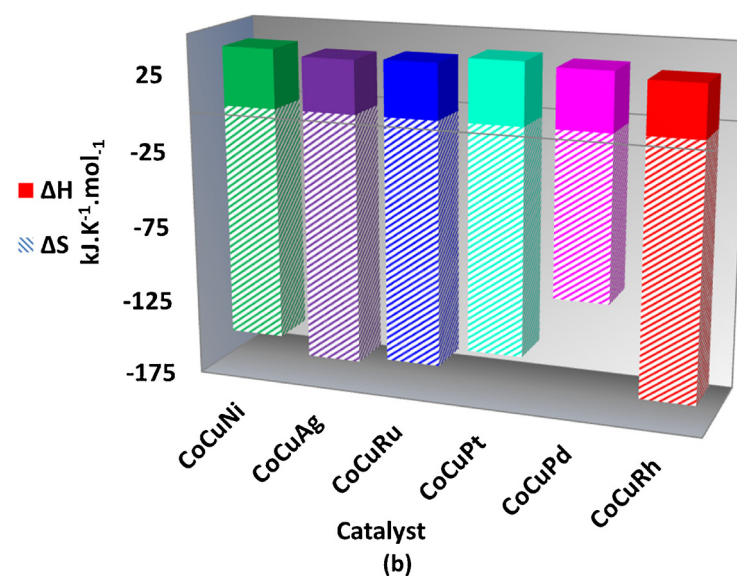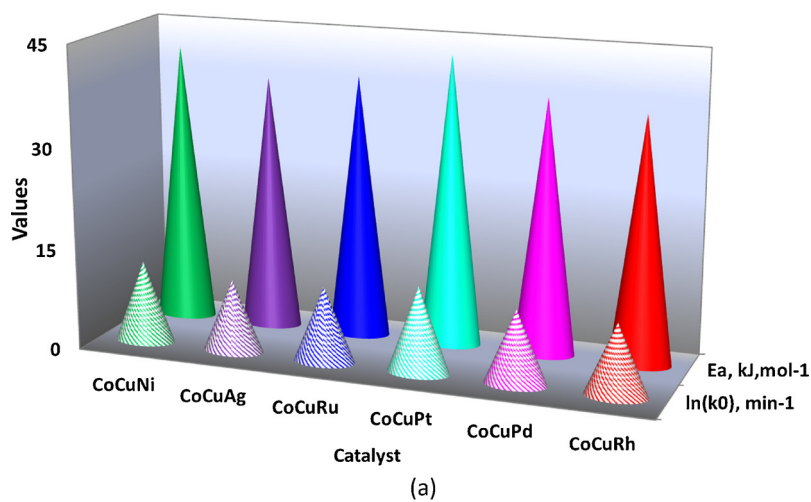

Fig. 6. Kinetic (a) and thermodynamic (b) assessment results for all metal promoted TMNPs.

energy barrier over which the reactants must past the form products while it never changes the equilibrium or end point of the reaction. Thus, thermodynamic values such as ΔH, ΔS and ΔG etc. for the reaction with or without a catalyst is always the same. Entropy is an instinct property of process which explained by the second law of thermodynamics to determine whether greater or less than zero. The negative values of $\Delta S^{\neq}$ and small values of $\Delta H^{\neq}$ implies that an associative mechanism occurs in the transition state for catalyzed NH_3BH_3 hydrolysis and the process is possible in nature [50,51].

The all thermodynamic and kinetic results reveal that addition of a promoter in the structure of CoCu NPs affected thermodynamic values. Rh was not only boosting the hydrogen evolution rate from 10.56 l H_2 min^{-1} g^{-1} to 13.92 l H_2 min^{-1} g^{-1}, but also decreasing the value of the E_a from 38.12 kJ mol^{-1} to 36.50 kJ mol^{-1} [21]. It means that only trace amount of Rh incorporated into NPs lowered the amount of required an external energy for starting hydrogen evolution and accelerated de bonding of hydrogen. In conclusion, hydrogen evolution was thermodynamically non-spontaneous when in the presence of TMNPs with lower activation energy.

With many solid catalyzed reactions, some general observations are considered out how catalyst promotes a reaction is not well understood, yet. In terms of transition state theory, the catalyst reduces the potential energy barrier and speeds up the reaction, while it never changes thermodynamics and the equilibrium constant of the reaction. In general, without catalyst the complex has high potential energy resulting in low rate reaction and with catalyst the lower energy barrier allows a higher rate of reaction by creating a different reaction paths from reactants to complex and from complex to products. In addition to these, the rate of heterogeneous reaction depends on surface kinetics, pore diffusion, particle ΔT, film ΔT and film diffusion resistance. To explain the action of catalysis, there are three main issues take into consideration: stoichiometry, kinetics and mechanism. Therefore, it is hardly possible to determine accurate correlation between rate and activation energy. For that reason, to make it clear we cannot any observed general observation between promoted catalysts. In our study, the highest hydrogen generation rate showed highest entropy change in addition to lowest activation energy observed in presence of CoCuRh catalyst. The comparison of the kinetic and thermodynamic values of all ternary catalysts were given in Fig. 6 a and b. Quite simply, CoCuRh TMNPs showed spectacular activity especially in comparison with Ni and Ag non-noble metals containing TMNPs, indicating the importance of addition of metal type into the CoCu structure. HER results showed that these metals slow down the reaction and classified as a negative catalyst for hydrolysis reaction [46].

Fig. 7 illustrates effect of promoting on hydrogen evolution activity in terms of rate constant as a function of BET specific surface area (a) and catalytic activity constant respect to CoCu NPs (b). It is well known that the surface area is the important parameter; affect the catalytic activity of the catalysis in hydrolysis. Although, it must be mentioned that the activity and surface area did not have direct or indirect proportion relation.

The obtained data was correlated with rate constant as shown in Fig. 7a. As can be seen the highest rate constant, achieved with CoCuRh TMNPs, exhibiting large surface area equal to 10.68 m^2 g^{-1}. The recorded surface area of CoCuRu TMNPs was the largest one among all the TMNPs and lower catalytic behavior displayed with lower rate constant. In agreement with previous studies, Ni containing catalyst showed higher specific areas than Co and Cu based catalysts [21,52]. The CoCuNi TMNPs showed an increase of almost 55% in BET surface area in comparison with CoCu suggestion positive effect when Ni was added into catalyst structure, despite showing low activity towards hydrogen generation by NH_3BH_3 hydrolysis [19,21]. In addition to this, we calculated catalytic activity constant (k/k_0) as the ratio of the rate constant (k) of the promoted-TMNPs reaction to the rate constant (k_0) of the CoCu NPs catalyzed reaction at specific temperature- 60 °C (see Fig. 7b). This constant, which indicated the most active catalyst was Rh

(a)

(b)
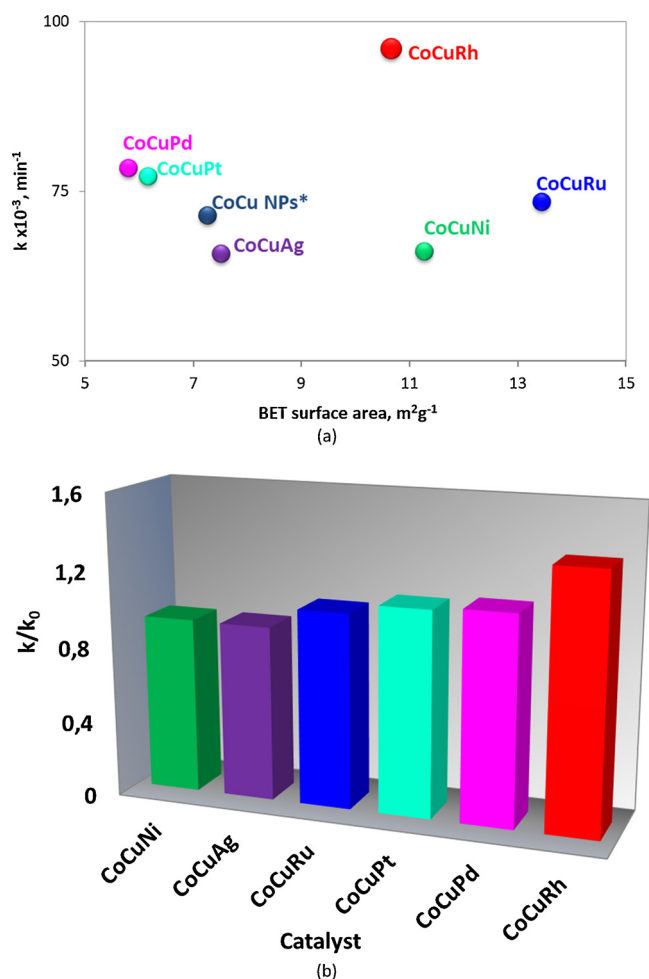
Fig. 7. Effect of promoting on hydrogen evolution activity: Rate constant as a function of BET specific surafec area (a), catalytic activity constant respect to CoCu NPs (b).

promoted TMNPs for this reaction.

General point of view in terms of promoting a catalyst by a metal addition describes as electronic effects, morphological effects, stabilizing effects, synergistic effects and bi-functional effects [53,54]. The morphological and structural properties of TMNPs were detailed as shown in Table 1 afforded to relevant results: (i) same crystalline oxide structures, (ii) mesoporous pore diameter, (iii) spherical morphology in nanometer scale, (iv) similar molar contents of metals, (v) CoCuRh TMNPs has the lower surface area than Ru and Ni promoted catalyst and higher surface area than Ag, Pt and Pd promoted catalysts, (vi) CoCuRh TMNPs has a bigger Co-Cu-O crystalline structure than CoCuNi TMNPs and smaller value of crystalline size than rest of TMNPs, (vii) Ru and Ni promoted TMNPs showed higher surface area than CoCuRh TMNPs and an apparent HER were lower than Rh promoted one. Despite of the fact that large surface leading to its highest HER of 21.21 l H_2 min^{-1} g$_{cat}^{-1}$ at 60 °C among the TMNPs catalysts, these results indicated that the morphological and structural properties have the limited influence on catalytic performance for NH_3BH_3 hydrolysis over synthesized TMNPs. A similar observation was also reported by several researcher [55–59].

The above results proved that the important of electronic changes on catalytic activity. The electronic influence is a dependent parameter that especially explains the interaction between band orbitals of the surface sites and molecular orbitals of reactants/products. A positive shift of 0.3-0.4 eV and 0.6-0.7 eV in corresponding BE peak of Co and Cu atoms, suggested electron transfer that all promoter affect the

electronic states of Co and Cu counterparts and led to electronic changes in CoCu TMNPs. These positive shifts were a signature of promoters in TMNPs electronic structure that caused to change in their catalytic activity. The aforementioned electronic structure results were strong evidence of electron transfer led to enhance the interaction between NPS and NH_3BH_3. This phenomena could be explain by different level of oxidation state of promoters, as both Rh and Pt have the same electronegativity of 2.28 eV but differ in oxidation state of Rh^{3+} (308.48 eV) and Pt^{2+} (316.78 eV) according to XPS. The electronegativity, which relates with electronic interaction influence the reaction rate, of an element increases with the oxidation state of the element [60–62]. The results indicated that NPs with higher electron negativity value was more catalytically active than lower ones.

It was mention that Ru could be separated from noble metal group, which include Pt, Rh and Pd, according to activity towards to NH_3BH_3 hydrolysis. To obtain the highest activity in NH_3BH_3 dehydrogenation, Rh must be a component of the mixture; in this sense Pt cannot replace with Rh. Also Chandra and Xu tested these metals for hydrolysis and they underlined that Ru showed less activity within noble metals and similar to non-noble metal behavior for this reaction [63]. Similar to this, our results showed that addition of Ru in to the CoCu structure did not improve the catalytic activity, significantly. The final demonstration that these factors are not solely affect the activity, the catalytic tests must be performed to find the activist promoter and in our study it is Rh.

3.4. Further characterization of Rh promoted CoCu TMPNs

3.4.1. Structural characterization

Further characterization results of Rh promoted CoCu TMNPs were shown in Fig. 8 as a sequence of TEM images at 200 nm (a) and 50 nm (b), particle size frequency (c), HRTEM images at 20 nm (d), SAED pattern (e), adsorption/desorption isotherm (f). The consequences of hydrogen evolution during NH_3BH_3 hydrolysis over TMNPs approved

that CoCuRh TMNPs showed improved catalytic activity. Furthermore characterization of CoCuRh TMNPs were carried out with the purpose to investigate whether and how catalyst activity dependence on internal and external properties. The detailed morphological features and particle size of CoCuRh TMNPs were further investigated by TEM analysis (Fig. 8a and b). The CoCuRh TMNPs of nm size spherical shape were obtained as shown in the histogram (Fig. 8c). Although most particles of 42 ± 18 nm were still present, also some particles were smaller than 20 nm. HRTEM (Fig. 8d) and corresponding SAED (Fig. 8e) images of CoCuRh TMNPs confirms that successful Rh promoting on the alloy structure rather than a mixture. Also homogeneous distribution of Rh confirm the alloy structure. The d-spacing (nm) indexed with red spots in SAED image (see inset Fig. 8e) revealed that 0.4624 nm, 0.4582 nm, 0.2837 nm, 0.2411 nm of (111), (111), (220), (311) spinel planes of the cobalt cupper oxide crystalline phase. The diffraction spots of (111), (200), (311) were observed at 0.2818 nm, 0.2427 nm, 0.1507 nm clearly indicated the distribution of Rh atoms.

The nitrogen adsorption-desorption isotherm of CoCuRh TMNPs could be ascribed to type-IV isotherms (Fig. 8f) supporting the presence of mesopores structure [36]. Mesopore-size distributions were determined by using the BJH method from the adsorption isotherm (Fig. S3) that exhibited distributions with the pore size centred at about 4 nm, suggesting the existence of mesopores [19]. Combined with the SEM and TEM results, sol-gel nitrate combustion prepared Rh promoted CoCu catalyst were nano sized spheres with mesoporous structure.

3.4.2. Bimolecular reaction mechanism investigation

The bimolecular reaction mechanism approach outlined above for a simple hydrolysis reaction could be generalized to much more complex reaction networks. There is a still gap of understanding the synergistic effect existing between Rh and Co-Cu structures for hydrogen evolution. Moreover this, previous studies proved that promoting has remarkable effect on the activity. The effective electron and mass transfer systems provided to develop bimolecular interaction and this resulted with
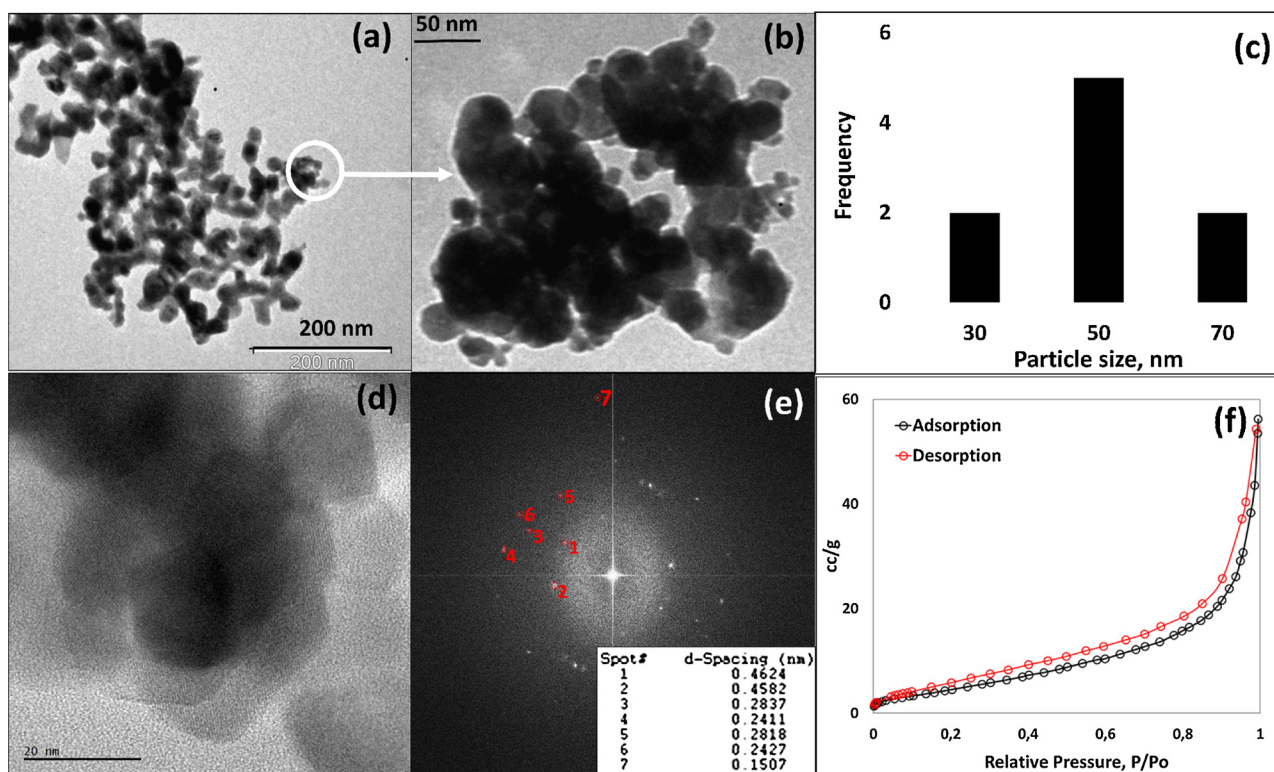

Fig. 8. Further characterizations of Rh promoted CoCu TMNPs: TEM images at 200 nm (a) and 50 nm (b), particle size frequency (c), HRTEM images at 20 nm (d), SAED pattern (e), adsorption isotherm (f).
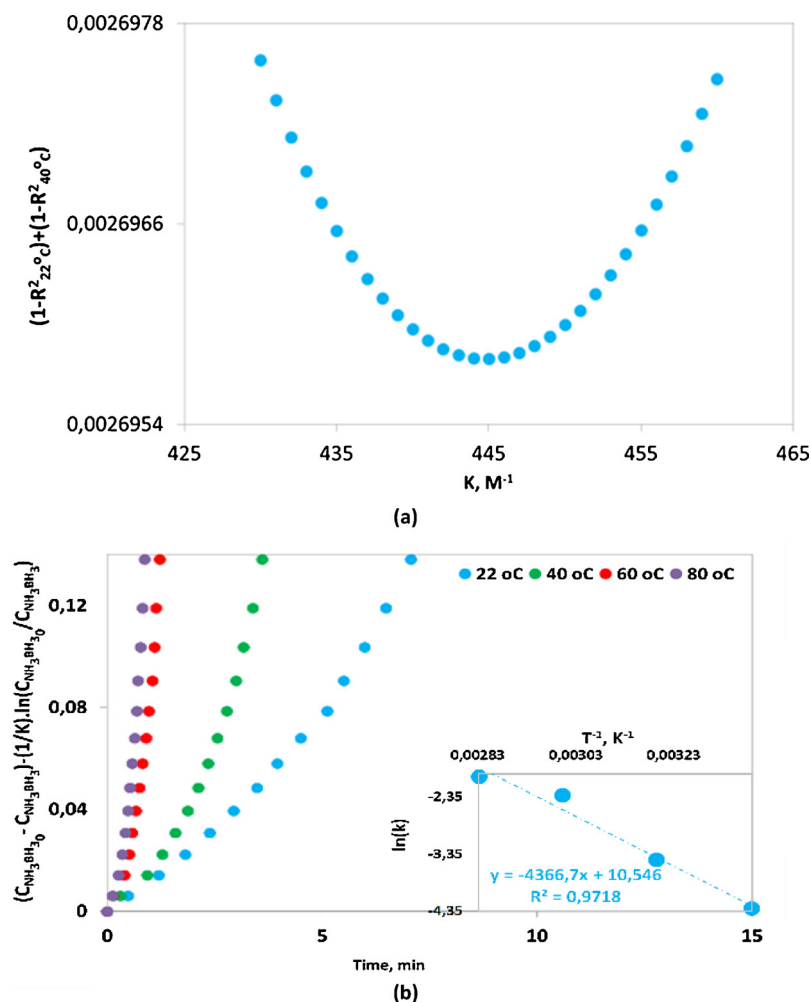
Fig. 9. Bimolecular kinetic investigations of Rh promoted CoCu TMNPs: Determination of K_a (a), L-H kinetic model graphics (b), Arrhenius graphics for L-H kinetic model (inset).

highly efficient reaction mechanism [46].

Fig. 9 illustrated bimolecular kinetic investigations results of Rh promoted CoCu TMNPs. The hydrogen evolution from NH_3BH_3 involved two important steps, as adsorption of NH_3BH_3 species and forming of hydrogen, which assumed a liquid phase reaction on a solid catalyst surface. The using of L-H bimolecular reaction mechanism provided more information about interaction about adsorption steps (Fig. 9a). As could be noted that promoting CoCu TMNPs by using Rh metal counterparts, the K_a value was increased to 455 M^{-1} compared with CoCu NPs (204 M^{-1}), Co NPs (108 M^{-1}) and Cu NPs (28 M^{-1}). It could be deduced from the K_a values that synergism increased by each part addition, as a consequence of this adsorption escalated and HER activation increased with directly proportion by improving of interaction between TMNPs and NH_3BH_3 [19,21]. Arrhenius plots of L-H reaction mechanism (Fig. 9b and inset) use for the calculation of E_a values for the hydrolysis reaction as 36.30 kJ mol^{-1} as comparable with the results of zero-order model approach.

In order to explain the hydrolysis process at microscopic level, it was proposed that two possible reaction pathways for NH_3BH_3 adsorption process for activation of B–N bonds. The first pathway corresponded to activation of protons and second one described the activation of both water and NH_3BH_3 molecules [64]. The H_2O molecules reacted with NH_3BH_3 and, intermediates fully hydrolyzed to evaluate three molecules of hydrogen and by-products in the form of H−B−O, and N−H−O. When catalyst was added, the reaction pathway clearly changed corresponding with lower E_a from the respective of proposed

mechanism a same hypothesis was previously reported based on transition state theory.

3.4.3. Reusability, recyclability, stability of CoCuRh in the hydrolysis of NH_3BH_3

Reusability, recyclability and stability play an important role in order to design an active and efficient catalyst (Fig. 10). These are important criteria for judging the catalytic performance, which are generally determined relative activity maintained in runs of catalytic reaction carried out by using the same catalyst after each run. During these tests, isolation of catalyst could lead to loss of catalytic materials and time. These problems could be solving by using magnetically isolable catalysts. Magnetically separable property provided an easily control of hydrogen evolution by altering the contact ratio of TMNPs with reaction medium. Although HER decreased by runs, over 99% conversion of NH_3BH_3 was obtained in all runs of these tests, i.e. releasing 3.0 equivalent H_2 per mol of NH_3BH_3. As could be clearly seen the reaction kinetic investigation results in Table 3, HER was much less dependent on NH_3BH_3 concentration in reusability, recyclability in general but nevertheless it did not follow zero-order kinetics due to the interactions between the catalysts and OH/H_2O after ≥3rd run in stability tests and ≥9th run in reusability tests.

Fig. 10 shows the comparisons of CoCuRh TMNPs in terms of catalytic activity sustained after multiple runs in hydrolysis of NH_3BH_3. The hydrogen evolution started immediately without noticeable induction period and proceed until the consumption of all NH_3BH_3. The
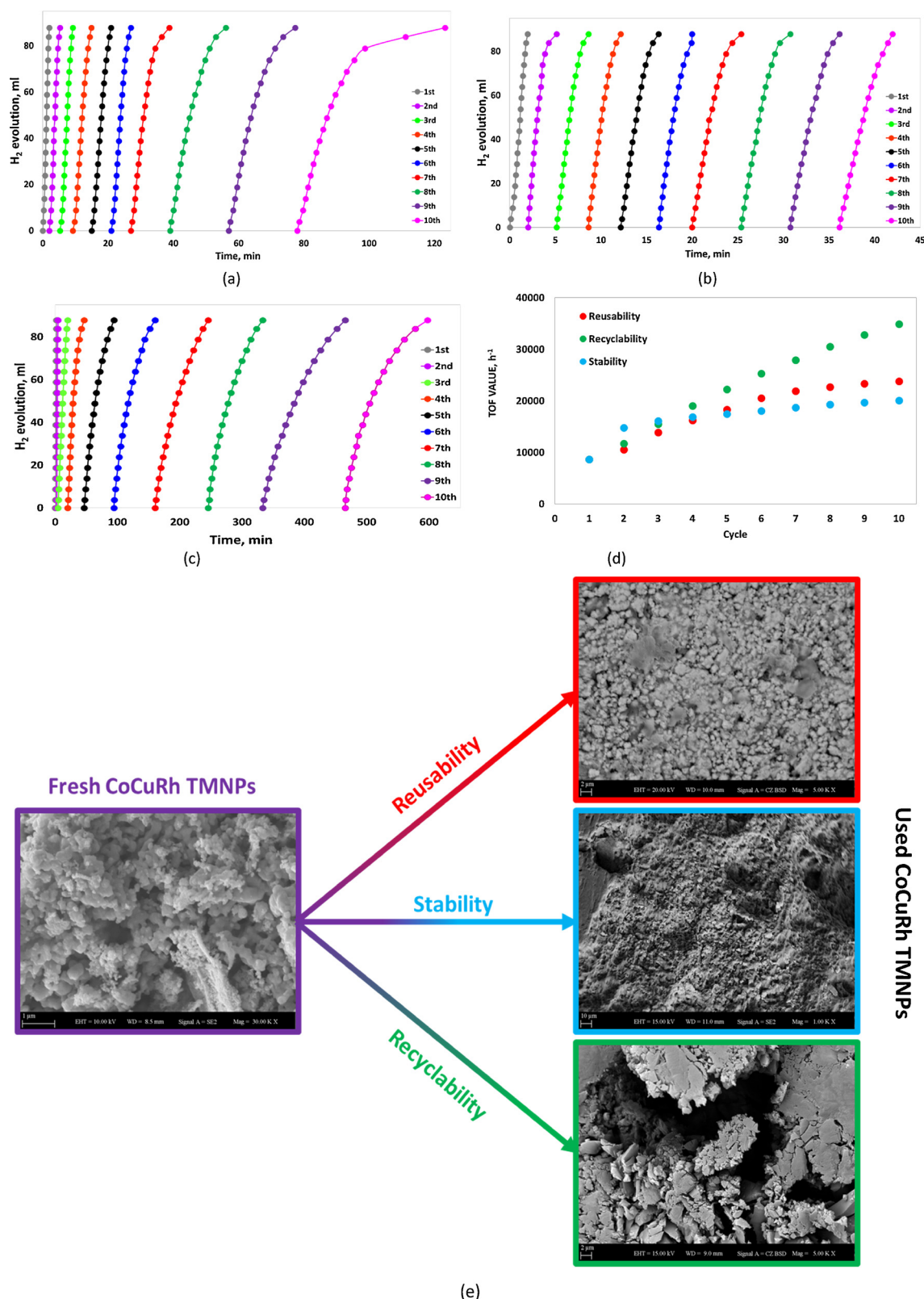
Fig. 10. Reusability (a), recyclability (b), stability (c) performances, turnover frequency (d) results and SEM images of fresh and used of Rh promoted CoCu TMNPs (e).

reusability of CoCuRh TMNPs showed an activity could be further maintained and easily reused again after simple washing procedure for 10 runs without obvious deactivation (Fig. 10a). In the recyclability tests, CoCuRh TMNPs retained its performance and interaction behavior with reactants (Fig. 10b). The stability results of CoCuRh TMNPs revealed that hydrogen evolution from NH_3BH_3 after keeping for 3 months in the hydrolysis spent solution could be achieved, the HER could be controllable, and TMNPs could be separable and reused again (Fig. 10c).

CoCuRh TMNPs comparison of performance had seldom been

Table 3

R^2 values of power law models for reusability, recyclability, stability performances at 0.12 M NH_3BH_3 solution, 5 mg TMPNs, 60 °C and 750 rpm (The best fitting model was indicated by bold characters).

Number of usage	Reusability			Recyclability			Stability		
	0	1	2	0	1	2	0	1	2
1	**0.9955**	0.9747	0.6593	**0.9965**	0.9080	0.6754	**0.9943**	0.8868	0.6415
2	**0.9931**	0.9385	0.7227	**0.9925**	0.9511	0.7418	**0.9844**	0.9715	0.7823
3	**0.9984**	0.9298	0.7070	**0.9970**	0.9601	0.7596	0.9323	**0.9990**	0.8814
4	**0.9932**	0.9551	0.7502	**0.9909**	0.9612	0.7609	0.9751	**0.9811**	0.8058
5	**0.9974**	0.9273	0.7027	**0.9968**	0.9446	0.7290	0.9734	**0.9817**	0.8063
6	**0.9944**	0.9523	0.7454	**0.9868**	0.9687	0.7772	0.9760	**0.9803**	0.8034
7	**0.9819**	0.9747	0.7923	**0.9878**	0.9652	0.7701	0.9711	**0.9822**	0.8078
8	**0.9785**	0.9768	0.7938	**0.9912**	0.9597	0.7598	0.9663	**0.9669**	0.7698
9	0.9565	**0.9837**	0.8135	**0.9932**	0.9548	0.7459	0.9706	**0.9838**	0.8126
10	0.9723	**0.9930**	0.8477	**0.9929**	0.9570	0.7526	0.9633	**0.9889**	0.8323

evaluated under standard conditions under three different operation conditions. To make comparison, TOF values were calculated for each cycle and illustrated in Fig. 10d. It must be noted that decrease in catalytic hydrogen evaluation activity of stability performance showed the lowest endurance, despite recyclability performance showed higher performance profile. Consequence usage of same TMNPs by only adding reactant NH_3BH_3 provided much better ease of handling. Also it must be recognized that during isolation of TMNPs could be lead to significant loss of the catalytic activity in reusability performances. During stability performance, by-products could be immersed on the active sites and led to faster deactivation [65].

The effect of the reusability, recyclability, and stability performances on surface properties of fresh catalysts, isolated from the 10th spent reaction solution, were evaluated by SEM analyses as given Fig. 10e. The deactivation of catalyst during AB hydrolysis occurred due to adsorption of B-containing species and particle agglomerations [36,66,67].

Both used catalysts contained a certain amount of agglomerations with irregular shapes compared with fresh catalysts. It is worth to mention that, the used catalyst showed a lower tendency towards agglomeration into larger NPs and had size distributions similar to the fresh catalysts after reusability performances compared with used catalysts after recyclability and stability performances. Larger particles with more significant agglomeration of smaller sized particles and changed in particle size of NPs was draw attention in used catalysts (see Fig. 10e). That was the main reason of the lower activity after the recyclability and stability performances. At these tests, catalysts were not washed after each cycle, which led to deposit of B-containing species on the surface.

3.4.4. Effect of NH_3BH_3 concentration and catalyst dosage

For better understanding of the effect of NH_3BH_3 concentration and catalyst dosage on hydrogen evolution performance, series of experiments in presence of CoCuRh TMNPs were carried out at a temperature of 60 °C (Fig. 11).

The reactivity of the CoCuRh TMNPs was explored at four different NH_3BH_3 concentration corresponding to constant NH_3BH_3 and catalyst dosage (5 mg) by only altering water quantity in the hydrolysis medium (Fig. 11a). The all HE performances started immediately and continued up to complete consumption of NH_3BH_3. HER activities was obtained in order of 0.48 M > 1.2 M > 0.24 M > 0.12 M NH_3BH_3. As can be seen from Fig. 11a, hydrogen evolution profiles of 0.12 M and 0.24 M NH_3BH_3 showed similar behaviors also their HER values. Comparably, catalyst was also performed almost same behaviors for 0.48 M and 1.2 M NH_3BH_3 except a certain point. The small decrease in HER and slowing downtowards the end of the reaction at 1.2 M could be related with the increase in viscosity of reaction solution due to the increasing substrate concentration and inevitably retard mass transfer [15].

Evoluted hydrogen volume was plotted versus time and the result

was a straight line. This mean that a rate was independent of the concentration of the reactant(s). Under our experimental conditions, it could be concluded that HER tendency could be separated into two: at low concentration (0.12 M-0.24 M NH_3BH_3) and high concentration (0.48 M–1.2 M NH_3BH_3). In both groups, hydrogen evolution behaviors were similar and linearly. Under certain ratios of catalyst to NH_3BH_3, HE performance in connection with zero-order power law kinetic (Also see R^2 values in Table 4).

Further studies were performed using CuCuRh TMNPs in different catalyst dosage at 60 °C. Fig. 11b shows the plots of hydrogen volume and inset also shows the HER values as a function of time and catalyst dosage, respectively. Generally, without a noticeable induction period and continues almost linearly until all NH_3BH_3 was consumed. Equivalent amount of hydrogen were achieved in a shortest time, when the 10 mg catalyst used. A similar observation was made in the CoCuRh TMNPs dosage scanning, wherein 2.5 mg CoCuRh TMNPs exhibited higher activity than lower as well as higher mass, the reactivity trend being in terms of mass of CoCuRh TMNPs to NH_3BH_3 was 0.0672 (2.5 mg) > 0.1344 (5 mg) > 0.0336 (1.25 mg) > 0.2688 (10 mg), which followed the same trend for NH_3BH_3 concentration. However, these trends needed to be interpreted with interaction of NH_3BH_3 and CoCuRh TMNPs in the hydrolysis reaction. The maximum hydrogen evolution rate was reached to 21.21 l H_2. g^{-1}cat. min^{-1} in presence of 2.5 mg Rh promoted CoCu TMNPs. Table 4 listed the value of R^2 given for 60 °C and 750 rpm at different NH_3BH_3 concentration and CoCuRh TMNPs dosage. It was seen that NH_3BH_3 hydrolysis obeyed the zero-order kinetic model as mentioned at Section 3.3. This means that hydrolysis reaction occurred on the surface of TMNPs and independent from AB concentration in reaction medium. Also ratio of NH_3BH_3 to catalyst was an important factor, by increasing it the time for completion of reactions decreases, despite reactivity have a limitation as could be seen from results.

4. Conclusion

In summary, a series of CoCu based ternary metal nanoparticle catalysts within mesoporous were prepared by addition of only certain amount of metal promoter as noble and non-noble metlas to Co-Cu sol to boost the activity. The effects of third metal in the structure were also carefully studied and explained in order to illuminate the effect on the physical and chemical properties changes. The characterization results revealed that these properties had a limited influence on catalytic activity and the more important parameters was electronic structure of synthesized TMNPs. In fact a very small amount of a platinum metals led to synergism and enhanced the activity of nanoparticles. It was worth noting that these non-noble metal promoted CoCu TMNPs exhibited much lower activity than noble metal promoted NPs. By varying the third metal in structure of CoCu based catalysts, it was found that catalytic activity of 13.92 l H_2. g^{-1}cat. min^{-1} HGR exhibit maximum
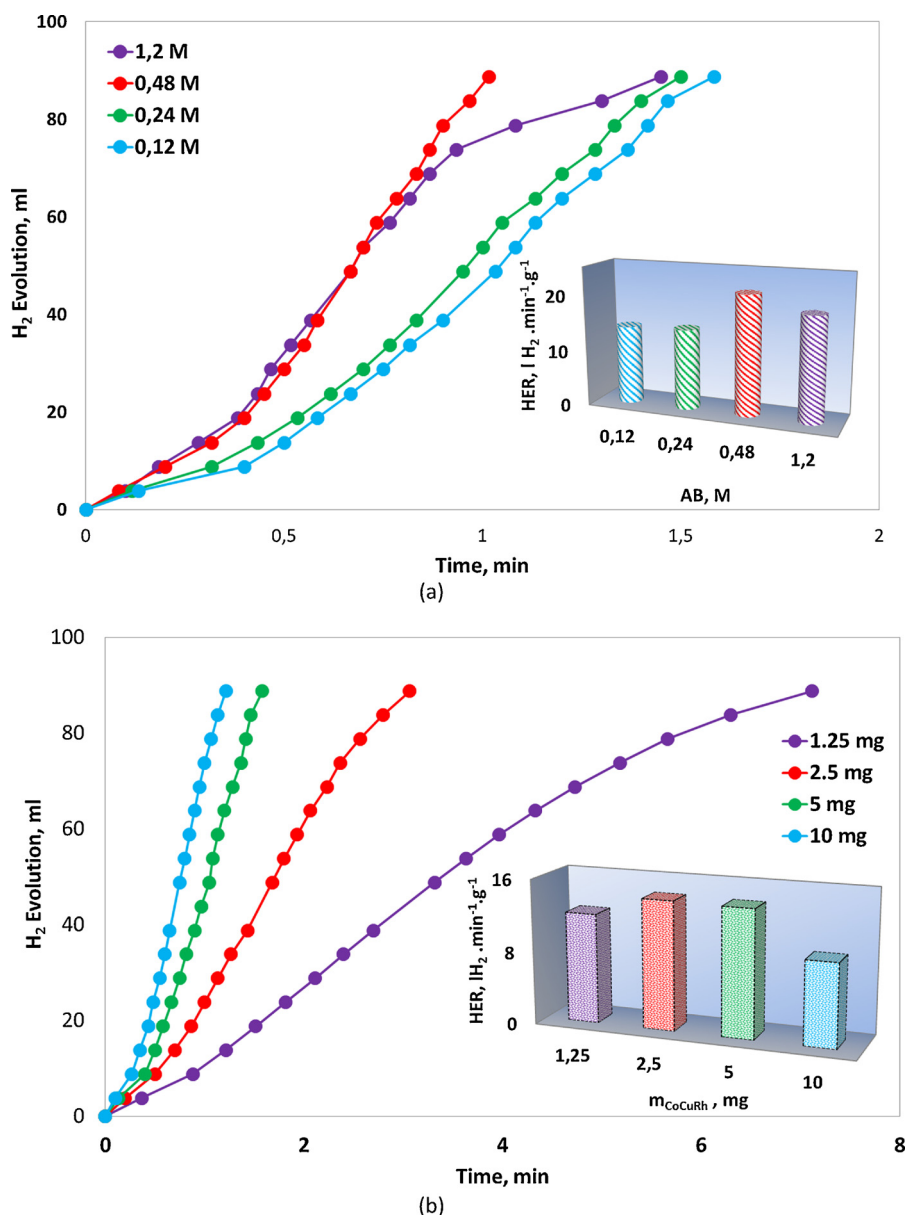
Fig. 11. Effect of NH_3BH_3 concentration (a) and catalyst dosage on H_2 evolution over Rh promoted CoCu TMNPs at 60 ^{0}C.

Table 4
Effect of NH_3BH_3 concentration and CoCuRh TMNPs dosage on degree of NH_3BH_3 hydrolysis, R^2 values given for 60$^°$C and 750 rpm (The best fitting model was indicated by bold characters).

Parameters	Value	R^2 values of nth degree Power Law Models for 60°C		
		0.	1.	2.
[AB], M	0.12	**0.9957**	0.8997	0.6605
5 mg CoCuRh	0.24	**0.9914**	0.8922	0.6541
	0.48	**0.9782**	0.8586	0.6126
	1.20	**0.9894**	0.9284	0.7765
CoCuRh, mg	1.25	**0.9950**	0.9546	0.7487
0.12 M AB	2.50	**0.9981**	0.9241	0.6991
	5.00	**0.9910**	0.8960	0.6680
	10.00	**0.9951**	0.9001	0.6640

enhancement with Rh addition. The superior HER has been demonstrated by optimizing the dehydrogenation conditions, the enhanced reaction rate was reached to 21.21 l H_2. g^{-1}cat. min^{-1} by optimizing the reaction conditions. We think that CoCuRh ternary metal nanoparticle catalyst will impact the hydrogen production aspects in the upcoming years by developing highly efficient and cost-effective catalyst with low noble metal promoting and easy production approach.

Appendix A. Supplementary data

Supplementary material related to this article can be found, in the online version, at doi:https://doi.org/10.1016/j.apcatb.2018.07.031.

References

[1] X. Qiao, L. Niu, H. Zhang, X. Wen, Y. Cao, G. Bai, Controllable fabrication of a novel porous Ni-alginate hybrid material for hydrogenation, Appl. Catal., B. 218 (2017)

721–730.

[2] O. Levenspiel, Chemical Reaction Engineering, third edition, Wiley, USA, 1999.

[3] H.S. Fogler, Elements of Chemical Reaction Engineering, fourth edition, Pearson Education International, Tenth printing, Massachusetts, USA, 2010 February.

[4] P. Rylander, Catalytic Hydrogenation Over Platinum Metals, Elsevier, 2012.

[5] N. Yan, L. Lingwen, Y. Jinyun, L. Yue-jian, W. Lin-hong, Y. Jinlong, W. Zhikun, Bimetal doping in nanoclusters: synergistic or counteractive? Chem. Mater. 28 (2016) 8240–8247.

[6] C. Wang, E. Sasmaz, C. Wen, J. Lauterbach, Pd supported on $SnO_2 - MnO_x - CeO_2$ catalysts for low temperature CO oxidation, Catal. Today 258 (2015) 481–486.

[7] H. Chen, Z. Ye, X. Cui, J. Shi, D. Yan, A novel mesostructured alumina−ceria−zirconia tri-component nanocomposite with high thermal stability and its three-way catalysis, Microporous Mesoporous Mater. 143 (9) (2011) 368–374.

[8] H. Liu, Y. Zheng, G. Wang, S. Qiao, A Three-component nanocomposite with synergistic reactivity for oxygen reduction reaction in alkaline solution, Adv. Energy Mater. 5 (1401186) (2015) 1–7.

[9] J. Zhang, K. Li, B. Zhang, Synthesis of dendritic Pt−Ni−P alloy nanoparticles with enhanced electrocatalytic properties, Chem. Commun. 51 (2015) 12012–12015.

[10] R. Fernandes, N. Patel, A. Paris, L. Calliari, A. Miotello, Improved H_2 production rate by hydrolysis of Ammonia Borane using quaternary alloy catalysts, Int. J. Hydrogen Energy 38 (8) (2013) 3313–3322.

[11] N. Patel, R. Fernandes, G. Guella, A. Miotello, Nanoparticle-assembled Co-B thin film for the hydrolysis of ammonia borane: a highly active catalyst for hydrogen production, Appl. Catal. B 95 (2010) 137–143.

[12] T. Liu, J. Yu, H. Bie, Z. Hao, Highly efficient hydrogen generation from hydrous hydrazine using a reduced graphene oxide-supported NiPtP nanoparticle catalyst, J. Alloys Compd. 690 (2017) 783–790.

[13] F. Song, W. Li, Y. Sun, Metal–organic frameworks and their derivatives for photocatalytic water splitting, Inorganics. 5 (40) (2017) 1–15.

[14] J.A. Turner, Sustainable hydrogen production, Science 305 (2004) 972.

[15] D. Özhava, N.Z. Kılıçaslan, S. Özkar, PVP-stabilized nickel(0) nanoparticles as catalyst in hydrogengeneration from the methanolysis of hydrazine boraneor ammonia borane, Appl. Catal. B 162 (2015) 573–582.

[16] Z. Guo, T. Liu, Q. Wang, G. Gao, Construction of cost-effective bimetallic nanoparticles on titanium carbides as a superb catalyst for promoting hydrolysis of ammonia borane, RSC Adv. 8 (2) (2018) 843–847.

[17] A. Kantürk Figen, Dehydrogenation characteristics of ammonia borane via boron-based catalysts (Co–B, Ni–B, Cu–B) under different hydrolysis conditions, Int. J. Hydrogen Energy 38 (22) (2013) 9186–9197.

[18] Q. Xu, M. Chandra, A portable hydrogen generation system: catalytic hydrolysis of ammonia–borane, J. Alloys Compd. 446 (2007) 729–732.

[19] B. Coşkuner Filiz, S. Pişkin, Investigation on activities of metal oxides catalyzed ammonia borane hydrolysis, Sigma 34 (2) (2016) 159–173.

[20] J. Sun, W. Niu, A. Taguchi, Ta. Abe, Y. Yoneyama, N. Tsubaki, Combining wet impregnation and dry sputtering to prepare highly-active CoPd/H-ZSM5 ternary catalysts applied for tandem catalytic synthesis of isoparaffins, Catal. Sci. Technol. 4 (2014) 1260–1266.

[21] B. Coşkuner Filiz, A. Kantürk Figen, S. Pişkin, Dual combining transition metal hybrid nanoparticles for ammonia borane hydrolytic dehydrogenation, Appl. Catal. A 550 (2018) 320–330.

[22] F.-Z. Song, Q.L. Zhu, X.-C. Yang, Q. Xu, Monodispersed CuCo nanoparticles supported on diamine-functionalized graphene as a non-noble metal catalyst for hydrolytic dehydrogenation of ammonia borane, Chem. Nano. Mater. 2 (2016) 942–945.

[23] F.-Z. Song, Q.-L. Zhu, X. yang, W.-W. Zhan, P. Pachfule, N. Tsumori, Q. Xu, metal–organic framework templated porous carbon-metal oxide/reduced graphene oxide as superior support of bimetallic nanoparticles for efficient hydrogen generation from formic acid, Adv. Energy Mater. 8 (1701416) (2018) 1–5.

[24] P. Verma, K. Yuan, Y. Kuwahara, K. Mori, H. Yamashita, Enhancement of plasmonic activity by Pt/Ag bimetallic nanocatalyst supported on mesoporous silica in the hydrogen production from hydrogen storage material, Appl. Catal. B 223 (2018) 10–15.

[25] M. Navlani-Garcia, K. Mori, Y. Kuwahara, H. Yamashita, Recent strategies targeting efficient hydrogen production from chemical hydrogen storage materials over carbon-supported catalysts, NPG Asia Mater. 1 (2018).

[26] Z. Huang, T. Autrey, Boron–nitrogen–hydrogen (BNH) compounds: recent developments in hydrogen storage, applications in hydrogenation and catalysis, and new syntheses, Energy Environ. Sci. 5 (2012) 9257–9268.

[27] Y. Jia, R. Hu, Q. Zhou, H. Wang, X. Gao, J. Zhang, Boron-modified activated carbon supporting low-content Au-based catalysts for acetylene hydrochlorination, J. Catal. 348 (2017) 223–232.

[28] A.P. Grosvenor, M. Biesinger, R.StC. Smart, N.St McIntyre, New interpretations of XPS spectra of nickel metal and oxides, Surf. Sci. 600 (9) (2006) 1771–1779.

[29] D. Lützenkirchen-Hecht, H.H. Strehblow, Anodic silver (II) oxides investigated by combined electrochemistry, ex situ XPS and in situ X-ray absorption spectroscopy, Surf. Interface Anal. 41 (2009) 820–829.

[30] D.J. Morgan, Resolving ruthenium: XPS studies of common ruthenium materials, Surf. Interface Anal. 47 (2015) 1072–1079.

[31] H. Chen, X. Zhang, J. Zhang, Q. Wang, Tuning decarboxylation selectivity for deoxygenation of vegetable oil over Pt-Ni bimetal catalysts via surface engineering, Catal. Sci. Technol. 8 (2018) 1126–1133.

[32] Y. Wang, Y.G. Nie, J.S. Pan, L.K. Pan, Z. Sun, L.L. Wanga, C.Q. Sun, Orientation-resolved 3d5/2 binding energy shift of Rh and Pd surfaces: anisotropy of the skin-depth lattice strain and quantum trapping, Phys. Chem. Chem. Phys. 12 (2010) 2177–2182.

[33] A.B. Kroner, M.A. Newton, M. Tromp, A.E. Russell, A.J. Dent, J. Evans, Structural characterization of alumina-supported Rh catalysts: effects of ceriation and zirconiation by using metal–organic precursors, Chem. Phys. Chem. 14 (15) (2013) 3606–3617.

[34] J. Li, Q.L. Zhu, Q. Xu, Non-noble bimetallic CuCo nanoparticles encapsulated in the pores of metal–organic frameworks: synergetic catalysis in the hydrolysis of ammonia borane for hydrogen generation, Catal. Sci. Technol. 5 (1) (2015) 525–530.

[35] W.W. Zhan, Q.L. Zhu, Q. Xu, Dehydrogenation of ammonia borane by metal nanoparticle catalysts, ACS Catal. 6 (10) (2016) 6892–6905.

[36] C.C. Hou, Q. Li, C.J. Wang, C.Y. Peng, Q.Q. Chen, H.F. Ye, W.F. Fu, C.M. Che, N. López, Y. Chen, Ternary Ni–Co–P nanoparticles as noble-metal-free catalysts to boost the hydrolytic dehydrogenation of ammonia-borane, Energy Environ. Sci. 10 (2017) 1770–1776.

[37] W. Chen, D. Li, C. Peng, G. Qian, X. Duan, D. Chen, X. Zhou, Mechanistic and kinetic insights into the Pt-Ru synergy during hydrogen generation from ammonia borane over PtRu/CNT nanocatalysts, J. Catal. 356 (2017) 186–196.

[38] M. Rakap, Hydrogen generation from hydrolysis of ammonia borane in the presence of highly efficient poly(N-vinyl-2-pyrrolidone)-protected platinum-ruthenium nanoparticles, Appl. Catal. A 478 (2014) 15–20.

[39] C. Yao, L. Zhuang, Y. Cao, X. Ai, H. Yang, Hydrogen release from hydrolysis of borazane on Pt- and Ni-based alloy catalysts, Int. J. Hydrogen Energy 33 (2008) 2462–2467.

[40] Y. Ge, Z.H. Shah, X.J. Lin, R. Lu, Z. Liao, S. Zhang, Highly efficient Pt decorated CoCu bimetallic nanoparticles protected in silica for hydrogen production from ammonia borane, ACS Sustain. Chem. Eng. 5 (2) (2016) 1675–1684.

[41] H. Zhang, X. wang, C. Chen, C. An, Y. Xu, Y. Huang, Q. Zhang, Y. Wang, L. Jilao, H. Yuan, Facile synthesis of Cu@CoNi core-shell nanoparticlescomposites for the catalytic hydrolysis of ammonia borane, Int. J. Hydrogen Energy 40 (2015) 12253–12261.

[42] H. Wang, L. Zhou, M. Han, Z. Tao, F. Cheng, J. Chen, CuCo nanoparticles supports on hierarchically porous carbon as catalyst for hydrolysis of ammonia borane, J. Alloys Compd. 651 (2015) 382–388.

[43] X.J. Yang, F.Y. Cheng, Z.L. Tao, J. Chen, Hydrolytic dehydrogenation of ammonia borane catalyzed by carbon supported Co core-Pt Shell nanoparticles, J. Power Sources 196 (2011) 2785–2789.

[44] G.Z. Chen, S. Desinan, R. Rosei, F. Rosei, D.L. Ma, Synthesis of Ni-Ru alloy nanoparticles and their high catalytic activity in dehydrogenation of ammonia borane, Chem. Eur. J. 18 (2012) 7925–7930.

[45] X. Yang, F. Cheng, J. Liang, Z. Tao, J. Chen, $Pt_x Ni_{1-x}$ nanoparticles as catalysts for hydrogen generation from hydrolysis of ammonia borane, Int. J. Hydrogen Energy 34 (2009) 8785–8791.

[46] J. Manna, S. Akbayrak, S. Özkar, Palladium (0) nanoparticles supported on polydopamine coated CoFe2O4 as highly active, magnetically isolable and reusable catalyst for hydrogen generation from the hydrolysis of ammonia borane, Appl. Catal. B 208 (2017) 104–115.

[47] H. Durak, M. Gülcan, M. Zahmakıran, S. Özkar, M. Kaya, Hydroxyapatite-nanosphere supported ruthenium(0) nanoparticle catalyst for hydrogen generation from ammonia-borane solution: kinetic studies for nanoparticle formation and hydrogen evolution, RSC Adv. 4 (2014) 28947–28955.

[48] Ö. Metin, S. Özkar, Hydrogen generation from the hydrolysis of ammonia-borane and sodium borohydride using water-soluble polymer-stabilized cobalt(0) nanoclusters catalyst, Energy Fuels 23 (2009) 3517–3526.

[49] Ö. Metin, Ş. Şahin, S. Özkar, Water-soluble poly(4-styrenesulfonic acid-co-maleic acid) stabilized ruthenium(0) and palladium(0) nanoclusters as highly active catalysts in hydrogen generation from the hydrolysis of ammonia–borane, Int. J. Hydrogen Energy 34 (2009) 6304–6313.

[50] M. Yurderi, A. Bulut, İ. Efecan Ertas, M. Zahmakıran, M. Kaya, Supported copper–copper oxide nanoparticles as active, stable and low-cost catalyst in the methanolysis of ammonia–borane for chemical hydrogen storage, Appl. Catal. B 165 (2015) 169–175.

[51] A. Bulut, M. Yurderi, İ. Efecan Ertas, M. Celebi, M. Kaya, M. Zahmakıran, Carbon dispersed copper-cobalt alloy nanoparticles: a cost-effective heterogeneous catalyst with exceptional performance in the hydrolytic dehydrogenation of ammonia-borane, Appl. Catal. B 180 (2016) 121–129.

[52] Monica Munoz, Sonia Moreno, Rafael Molina, Synthesis of Ce and Pr-promoted Ni and Co catalysts from hydrotalcite type precursors by reconstruction method, Int. J. Hydrogen Energy 37 (2012) 18827–18842.

[53] B. Coqa, F. Figueras, Bimetallic palladium catalysts: influence of the co-metal on the catalyst performance, J. Mol. Catal. A Chem. 173 (2001) 117–134.

[54] D.M. Alonso, S.G. Wettstein, J.A. Dumesic, Bimetallic catalysts for upgrading of biomass to fuels and chemicals, Chem. Soc. Rev. 41 (2012) 8075–8098.

[55] J. Zhang, Y. Li, Y. Zhang, M. Chen, L. Wang, C. Zhang, H. He, Effect of support on the activity of Ag-based catalysts for formaldehyde oxidation, Sci. Rep. 5 (12950) (2015) 1–10.

[56] L. Pikna, M. Heželová, S. Demčáková, M. Smrčová, B. Plešingerová, M. Štefanko, M. Turáková, M. Králik, P. Puliš, P. Lehocký, Effect of support on activity of palladium catalysts in nitrobenzene hydrogenation, Chem Papers 68-5 (2014) 591–598.

[57] G. Sharma, D. Kumar, A. Kumar, A.H. Al-Muhtaseb, D. Pathania, M. Naushad, G.T. Mola, Revolution from monometallic to trimetallic nanoparticle composites, various synthesis methods and their applications: a review, Mater. Sci. Eng. C Mater. Biol. Appl. 71 (2017) 1216–1230.

[58] M. Chandra, Q. Xu, Room temperature hydrogen generation from aqueous ammonia-borane using noble metal nano-clusters as highly active catalysts, J. Power Sources 168 (2007) 135–142.

[59] N. Sadokhina, G. Smedler, U. Nylén, M. Olofsson, L. Olsson, The influence of gas composition on Pd-based catalyst activity inmethane oxidation − inhibition and

promotion by NO, Appl. Catal. B 200 (2017) 351–360.

[60] M.T. Greiner, L. Chai, M.G. Helander, W.-M. Tang, Z.H. Lu, Transition metal oxide work functions: the influence of cation oxidation state and oxygen vacancies, Adv. Funct. Mater. 22 (2012) 4557–4568.

[61] I. Najdovski, P.R. Selvakannana, A.P. O'Mullane, Electrochemical formation of Cu/Ag surfaces and their applicability as heterogeneous catalysts, RSC Adv. 4 (2014) 7207–72015.

[62] L. Hea, C. Liua, J. Tanga, Y. Zhoua, H. Yanga, R. Liua, J. Hua, Self-catalytic stabilized Ag-Cu nanoparticles with tailored SERS response for plasmonic photocatalysis, Appl. Surf. Sci. 434 (2018) 265–272.

[63] M. Chandra, Q. Xu, A high-performance hydrogen generation system: transition metal-catalyzed dissociation and hydrolysis of ammonia–borane, J. Power Sources 156 (2006) 190–194.

[64] L. Wang, H. Li, W. Zhang, X. Zhao, J. Qiu, A. Li, X. Zheng, Z. Hu, R. Si, J. Zeng, Supported rhodium catalysts for ammonia–borane hydrolysis: dependence of the catalytic activity on the highest occupied state of the single rhodium atoms, Angew. Chem. Int. Ed. 56 (2017) 1–7.

[65] A. Kantürk Figen, B. Coşkuner, A novel perspective for hydrogen generation from ammonia borane (NH₃BH₃) with Co–B catalysts:"Ultrasonic Hydrolysis", Int. J. Hydrogen Energy 38 (6) (2013) 2824–2835.

[66] W. Chen, X. Duan, G. Qian, D. Chen, X. Zhou, Carbon nanotubes as support in the platinum-catalyzed hydrolytic dehydrogenation of ammonia borane, Chem. Sustain. Chem. 8 (2015) 2927–2931.

[67] W. Chen, Z. Wang, X. Duan, G. Qian, D. Chen, X. Zhou, Structural and kinetic insights into Pt/CNT catalysts during hydrogen generation from ammonia borane, Chem. Eng. Sci. (2017), https://doi.org/10.1016/j.ces.2017.05.056.